Development ofanIntegrated Biophysical Modeltorepresentmorphological and ecological processes in a changing deltaic and coastal ecosystem

Article *in* Environmental Modelling and Software · September 2018

DOI: 10.1016/j.envsoft.2018.05.019

Ehab A. Meselhe
The Water Institute of the Gulf

Environmental Modelling and Software 109 (2018) 402–419

Contents lists available at ScienceDirect

Environmental Modelling & Software

journal homepage: www.elsevier.com/locate/envsoft

Development of an Integrated Biophysical Model to represent morphological and ecological processes in a changing deltaic and coastal ecosystem

Melissa M. Baustian[a,*], Ehab Meselhe[a,b], Hoonshin Jung[a], Kazi Sadid[a], Scott M. Duke-Sylvester[c], Jenneke M. Visser[c], Mead A. Allison[a,b], Leland C. Moss[a], Cyndhia Ramatchandirane[a], Dirk Sebastiaan van Maren[d,e], Michelle Jeuken[d], Sibel Bargu[f]

[a] The Water Institute of the Gulf, Baton Rouge, LA, USA
[b] Department of River-Coastal Science and Engineering, Tulane University, New Orleans, LA, USA
[c] University of Louisiana at Lafayette, Lafayette, LA, USA
[d] Deltares, Delft, Netherlands
[e] Environmental Fluid Mechanics, Delft University of Technology, Delft, Netherlands
[f] Department of Oceanography and Coastal Sciences, Louisiana State University, Baton Rouge, LA, USA

ARTICLE INFO

Keywords:
Hydrodynamics
Nutrient dynamics
Vegetation dynamics
Morphodynamics
Global change
Numerical modeling

ABSTRACT

Deltaic and coastal ecosystems are changing in response to natural and anthropogenic forces that require ecosystem-level restoration efforts to avoid habitat degradation or loss. Models that link ecosystem components of hydrodynamics, morphodynamics, nutrient and vegetation dynamics to represent essential processes and feedbacks are advancing the field of environmental modeling and are vital to inform coastal restoration decisions. An Integrated Biophysical Model was developed by creating a new vegetation dynamics component and linking it to other primary ecosystem components that included essential feedbacks. The model performance was evaluated by applying it to a deltaic ecosystem that included marshes and estuaries. The Integrated Biophysical Model output captured the general temporal and spatial environmental trends of key variables. This integrated model is capable to perform long-term simulations to assess responses of deltaic and coastal systems to global change scenarios and can be used to inform restoration strategies in ecosystems worldwide.

1. Introduction

Deltaic and coastal ecosystems worldwide are rapidly changing (Bianchi and Allison, 2009) because of natural and anthropogenic activities that produce stressors, such as increased nutrient runoff and eutrophication (Rabalais et al., 2009; Scheffer et al., 2001), rising relative sea levels due to eustatic change and subsidence processes (Douglas, 1991; Syvitski et al., 2009), as well as anthropogenic alterations to riverine sediment loads (Syvitski et al., 2005; Walling and Fang, 2003). Ecosystem response to these stressors include loss of species diversity (Hooper et al., 2012), an increase in harmful algal blooms (Anderson et al., 2002), estuarine and coastal bottom-water hypoxia (Diaz and Rosenberg, 2008; Turner and Rabalais, 1991), and geomorphological changes, such as wetland loss (Nicholls, 2004; Tweel and Turner, 2012). Ecosystem responses may also alter ecosystem services to humans (Barbier et al., 2011). Changes in ecosystems and its services command the attention of resource managers at agencies that need to make urgent decisions about initiating large-scale restoration projects (Aronson and Alexander, 2013; Calmon et al., 2011; Lü et al., 2012). Decision support tools, such as science-based numerical models, are helpful and needed for managers and planners (Savchuk et al., 2012). Numerical models can be used to quickly project possible outcomes arising from alternative restoration projects and allow for a science-based assessment of whether or not projects are likely to meet their intended goals (Boesch, 2006; Reis et al., 2015; van Maren and Cronin, 2016).

A comprehensive model of ecosystem dynamics is needed that extends the state-of-the-art in two strategic ways. The first advancement that is needed is development of a model that incorporates the components of hydrodynamics, morphodynamics, nutrient dynamics and vegetation dynamics. Previous models focused on a subset of these major components of a coastal ecosystem. Some studies focused on the interaction between the flow field and the morphologic processes (e.g., Edmonds and Slingerland, 2010; Yuill et al., 2016); while others focused on the interaction between hydrodynamics and vegetation dynamics (e.g., Collins et al., 2004; D'Alpaos et al., 2006), or

* Corresponding author. The Water Institute of the Gulf, 1110 River Road South, Suite 200, Baton Rouge, LA, 70802, USA.
E-mail address: mbaustian@thewaterinstitute.org (M.M. Baustian).

https://doi.org/10.1016/j.envsoft.2018.05.019
Received 6 June 2017; Received in revised form 25 April 2018; Accepted 22 May 2018
1364-8152/

hydrodynamics and nutrient dynamics (e.g., Das et al., 2011; Smits and van Beek, 2013; Wang et al., 2016). Many of these linked models represent two or three of the major components of the coastal ecosystem where only one vegetation species is represented (Alizad et al., 2016) or do not consider nutrient dynamics with morphodynamics and vegetation dynamics (Fagherazzi et al., 2012; Reyes et al., 2000). There are few to no current ecosystem models that couple all four components to represent dynamic biophysical interactions over time. The second advancement needed is to include feedbacks among the four main components representing a coastal ecosystem. The typical approach when modeling both physical and ecological processes is for information to flow in one direction, from the physical models to the ecological models. This is based on the assumption that ecological processes do not significantly influence the dynamics of physical systems. However, plants can alter physical processes in a number of ways. For example, ecological state variables, such as submerged or emergent vegetation, can affect hydrodynamics by influencing drag and circulation (Ganju et al., 2015), and in turn, hydrodynamics can influence vegetation by producing flooding and salinity regimes that may alter plant community composition. To incorporate these feedbacks, we designed a model to allow transfer of information from one model to influence the dynamics of the others. These feedbacks and components in a model are needed to better represent coastal ecosystems because the landscape is rapidly changing and coastal managers are being asked to make urgent decisions on protecting and restoring the coastlines.

The main objective for this study was to develop a validated, Integrated Biophysical Model that includes dynamic coupling and feedbacks to capture: (1) morphological evolution resulting from sediment deposition into wetland areas, (2) salinity and nutrient-related effects on wetland vegetation, soils, and the estuarine open water conditions, and (3) allow changes in nutrient and vegetation dynamics to affect hydrological and morphological dynamics. An integrated state-of-the-art modeling framework (Delft3D) was improved and applied to Mississippi River Deltaic Plain to represent the essential components of the ecosystem, including the hydrodynamics, morphodynamics, nutrient dynamics, and vegetation dynamics. The hydrodynamics and morphodynamics components were existing Delft3D models that were parameterized to represent local conditions. The nutrient dynamics were based on the Delft3D D-WAQ model with modified algorithms that better reflected the ecology of coastal Louisiana. The vegetation dynamics component was a combination of an existing Delft3D model and newly developed algorithms. The existing models are briefly described here since they are extensively covered in literature (Lesser et al., 2004; Smits, 2013; Smits and van Beek, 2013), while the newly developed vegetation dynamic component is described in detail (see also Supplementary Materials, including Fig. SM1

2. Development of Integrated Biophysical Model

2.1. Model component overview

Four main components represent the key receiving estuarine basin processes: hydrodynamics, morphodynamics, vegetation dynamics, and nutrient dynamics (Fig. 1). The hydrodynamics component simulated the water, salinity, and temperature fields driven by tides, river flows, and time- and space-varying wind. The morphodynamics component accounted for changes in riverine reaches, receiving basin elevation, and suspended sediment transport, including the deltaic growth and decay. Both the hydrodynamics and morphodynamics components influenced the nutrient dynamics component, which included the fate and transport of nutrients to open water, sediment/soil layers, and vegetated areas (submerged and emergent) of the receiving basin. The emergent vegetation component simulated the taxa distribution of the herbaceous marsh vegetation, nutrient uptake, and growth responses via allocation of above- and belowground biomass. The vegetation component influences the morphodynamics by trapping sediment while an increase in belowground biomass could additionally lead to an increase in bed levels. Components were integrated together to represent interactions and feedbacks for evaluating the performance of the Integrated Biophysical Model (Fig. 1). For example, the hydrodynamics and nutrient dynamics components were coupled for model assessment of nutrient dynamics. Morphodynamics component was assessed with the linked hydrodynamics component. The hydrodynamics, nutrient dynamics and vegetation dynamics components were all linked to calibrate and validate the wetland vegetation processes.

The Integrated Biophysical Model is composed of several Delft3D models that represent the main components. The hydrodynamics (D-FLOW) and morphodynamics (D-FLOW-SED-ONLINE) are computed with the Delft3D flow package, a widely used and well-validated open-source sediment transport model (Lesser et al., 2004). Nutrient dynamics, including nutrients and phytoplankton biomass were handled by D-WAQ of Delft3D. The existing vegetation biomass model (VEGMOD) within D-WAQ was modified extensively (see Table 1) to quantify wetland vegetation biomass changes and was coupled with two new vegetation models. One of the new models simulated changes in the taxa distribution of wetland vegetation (LAVegMod.DM) and the other captured the allocation of the above- and belowground biomass (LAVegMod.RootShoot). Finally, this Integrated Biophysical Model was developed and ran by an interdisciplinary team of scientists and engineers from various disciplines (ecology, geology, and hydrology).

The smaller grey boxes within the hydrodynamics, morphodynamics, nutrient and vegetation dynamics represent the essential variables (Fig. 1). Nutrient dynamics and vegetation biomass diagram was modified from Smits (2013). Dotted lines indicate that the coupling between components was newly developed, see Table 1.

2.2. General model set up

The model domain (80,800 km^2) and components were developed and applied to represent the lower Mississippi River and its estuarine receiving basins, all of which are located south of the City of New Orleans, LA, USA. The receiving basins, Barataria and Breton basins as well as the Mississippi River Delta are mainly composed of fresh to saline herbaceous wetlands with interspersed canals and estuarine shallow lakes and bays that drain into the northern Gulf of Mexico (GOM): see Fig. 2. Some of these estuarine open water areas are already eutrophic from nutrient sources that include local agricultural runoff, Mississippi River discharge and small, sediment-poor freshwater diversions (Caffrey and Day, 1986; Lane et al., 2007; Lundberg et al., 2014; Ren et al., 2009). The receiving basins are experiencing rapid and extensive wetland loss (Couvillion et al., 2011) that requires large-scale restoration efforts. Sustaining and creating new wetlands via placement of dredged material or proposed sediment diversions on the lower Mississippi River are proposed as large-scale restoration projects in *Louisiana's Comprehensive Master Plan for a Sustainable Coast* (Coastal Protection and Restoration Authority [CPRA], 2012).

To represent such a large spatial domain at tractable computational costs, the model landscape was subdivided into 14 domains using a domain decomposition technique, providing a flexible technique for local grid refinement. Complex flow fields (e.g., rapid changes to velocities) and significant morphological changes are expected to occur near the outfalls of the proposed sediment diversions, and therefore the resolution is highest here (100 × 100 m grid cells). The grid resolution was gradually reduced with increasing distance from these outfall areas. The total number of grid cells in the model is 334,685 and the largest grid cell size is 4 × 4 km. The model routines were developed in Fortran 90, Python, and C++, and individual model components were coupled by external MATLAB scripts (see Table 2).

Data sets from multiple sources were used to generate the bathymetry and topography for the hydrodynamic and morphological components. These included the 2012 Mississippi River channel multibeam bathymetry provided by the U.S. Army Corps of Engineers (USACE),

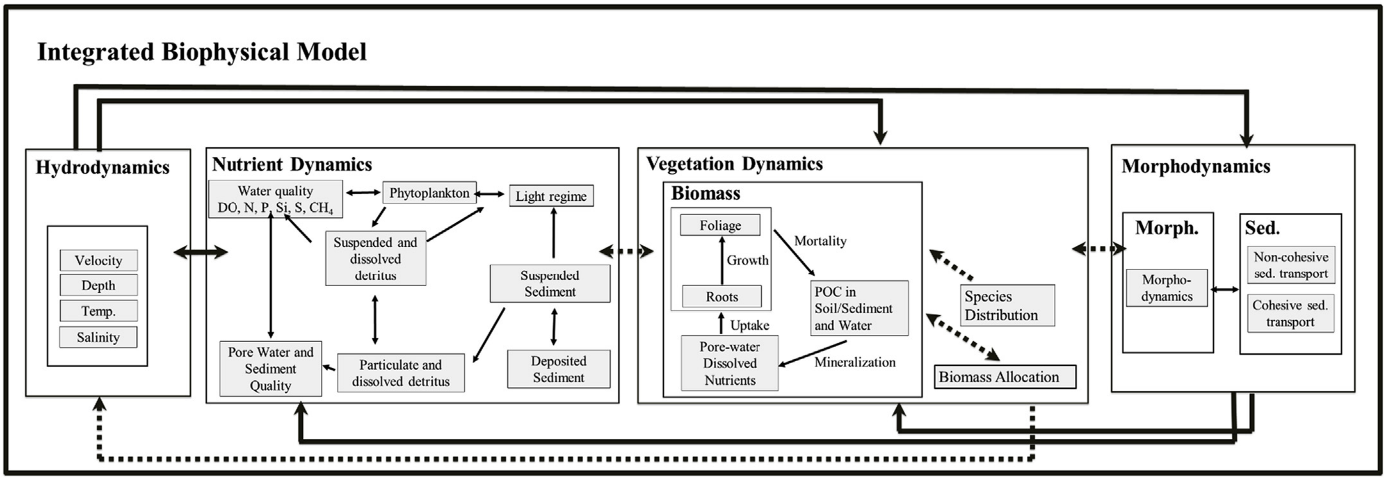

Fig. 1. Conceptual overview of the Integrated Biophysical Model that includes the feedbacks between components.

Table 1
Description of the development or modification of model components that make up the Integrated Biophysical Model that is run in the Delft3D environment. NA = not applicable.

Model Component	Model Name	Newly Developed? Y/N	Extensively Modified? Y/N	Reference
Hydrodynamics	D-FLOW-SED-ONLINE	N	N	Lesser et al., 2004
Nutrient Dynamics	D-WAQ	N	N	Smits 2013, Smits and van Beek, 2013
Vegetation Dynamics	LAVegMod.DM	N	Y	Visser et al., 2013
	LAVegMod.RootShoot	Y	NA	This study
	VEGMOD	N	Y	Smits 2013
Morphodynamics	D-FLOW-SED-ONLINE	N	N	Lesser et al., 2004

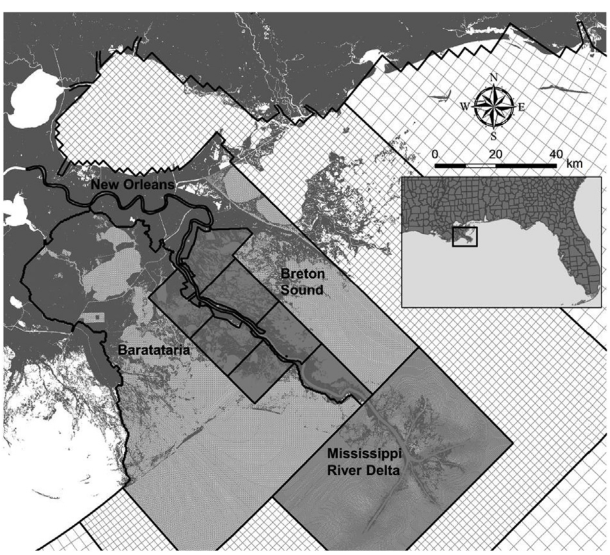

Fig. 2. Model domain composed of 14 subdomains that cover the Barataria and Breton Sound basins in the Mississippi River Deltaic Plain.

2012 LIDAR data of the Breton and Barataria basins provided by the U.S. Geological Survey (USGS), 2014 bathymetry data collected by the Water Institute of the Gulf for waterways within the Barataria and Breton receiving basins, and ADCIRC SL15v9 bathymetry data for the deeper GOM (e.g., shelf and slope) area. All bathymetry data were converted to the NAVD88 vertical datum expressed in meters (m)/geoid 12A. These 14 domains and underlying bathymetry were used by the hydrodynamic model to generate input for the nutrient dynamics, vegetation dynamics, and morphodynamics components of the model.

2.3. Feedbacks among coupled models

The feedback and dynamic coupling of the various modeling component is one of the key objectives of this effort to represent essential ecosystem processes that influence the landscape. The frequency of information passed among the coupled models depends on the nature of the ecosystem process (Table 2). For example, nutrient dynamics are simulated at a 10-min time step to reflect the time sensitivity of the biogeochemistry of the water and sediment/soils. On the other end of the spectrum, the spatial distribution of marsh vegetation is simulated at a one-year time step to reflect vegetation succession.

A sequence of events was developed to allow for information to be passed among the models in order to develop the Integrated Biophysical Model (see Supplementary Materials, Table SM2) - that had two main types of grid resolutions, the finer grid of the hydrodynamics model (HD grid) and the coarse grid of the nutrient dynamics model (ND grid). In the first step, the hydrodynamics and morphodynamics models calculated the parameters such as water elevation, velocity, salinity, temperature, sediment load and bed level changes (DEM change resulting from minerals contributions only). For Step 2, the water elevation and salinity information on the HD grid are passed to the vegetation species distribution model (LAVegMod.DM) that produces the vegetation spatial distribution for each vegetation taxa on the HD grid. The third step involves passing essential information to the nutrient dynamics model, which include all hydrodynamic information, including salinity and temperature and vegetation coverage on the HD grid that are then aggregated into the ND grid. The aggregated information is passed to nutrient dynamics model (D-WAQ) and vegetation dynamics model (VEGMOD) to simulate nutrient and vegetation biomass dynamics. Specifically, the vegetation dynamics model (VEGMOD) calculates the live and dead vegetation biomass with particulate organic matter (POM) in the soil layers. The next steps involve post-processing the information. In Step 4, the vegetation footprint

Table 2
Time steps for each model, the frequency of information that was passed to the next model, and if the coupling between models was new in the development of the Integrated Biophysical Model.

Model	Model Time Step		Provides Info to this Model	Frequency of Providing Information	Coupling New? Y/N
D-FLOW-SED-ONLINE	0.5 min	→	D-WAQ	10 min	N
D-FLOW-SED-ONLINE	1 min	→	LAVegMod.DM	1 year	N
LAVegMod.DM	1 year	→	D-WAQ	1 year	Y
LAVegMod.DM	1 year	→	D-FLOW-SED-ONLINE	1 year	Y
LAVegMod.DM	1 year	→	VEGMOD	1 year	Y
D-WAQ	10 min	→	LAVegMod.RootShoot	10 min	Y
D-WAQ	10 min	→	VEGMOD	10 min	N
LAVegMod.RootShoot	10 min	→	VEGMOD	10 min	Y
VEGMOD	10 min	→	D-FLOW-SED-ONLINE	1 year	Y

(e.g., wetland area) is adjusted by considering grid cells that only have live vegetation biomass that also influences the POM accumulation distribution caused by vegetation mortality.

2.4. Hydrodynamics component

The hydrodynamics component simulates the hydrodynamics on a curvilinear grid by solving unsteady shallow water equations in two dimensions (2D) or three dimensions (3D) (Lesser et al., 2004). The greatest emphasis in the Integrated Biophysical Model is on the relatively shallow (0–2 m) and vertically mixed water bodies and therefore the model is run in 2D depth-averaged mode (which means all variables are averaged over the water column). No storms, including pressure and waves were included in the model.

The hydrodynamics in the GOM were forced by 13 tidal constituents derived from Topex-Poseidon ocean surface elevation data (Egbert et al., 1994). Mississippi River inflow discharge was derived from the USGS gauge at Baton Rouge (USGS 07374000). The model also accounted for natural distributaries, smaller freshwater diversions (e.g., Bonnet Carré spillway, Caernarvon, and Davis Pond), in the lower Mississippi River, and for other rivers entering the modeled area (e.g., Amite, Tickfaw, Natalbany, Tangipahoa, Tchefuncte, Pearl, Pascagoula, and Mobile). Daily average water discharges were specified for these sources using data from the USGS gauging stations. Salinity time series boundary conditions were obtained from the National Oceanographic Data Center (NODC) Ocean Archive System (http://www.nodc.noaa.gov/cgi-bin/OC5/GOMclimatology/gomregcl.pl), and were enforced at the open boundaries of the GOM. A spatially and time-varying wind field (obtained from the National Oceanic and Atmospheric Administration (NOAA)-National Climatic Data Center (NCDC) data portal) was specified on a 5 × 5 km horizontal resolution. Water temperature was computed with the heat flux model (Ocean) in Delft3D-FLOW with a meteorological model driven by relative humidity, air temperature, and cloud coverage (NOAA portal) with a water temperature constant (25 °C) open water boundary condition. A spatially varying excess rainfall map was based on daily precipitation data (NOAA-based STAGE III River Forecast Center Operational NEXRAD database) and monthly average evaporation data (International Water Management Institute's World Water and Climate Data Atlas (IWMI, 2014).

A base roughness value was set up for the entire model domain (open water and marsh areas). The effect of vegetation-induced friction in the marsh was parameterized with an additional bed roughness term (added to the base roughness) (Baptist et al., 2007). This trachytope approach uses information on vegetation density (stem diameter x number of stems/area) and the fractional area (Fa) of a cell covered with vegetation (see Fig. 3). Vegetation distribution and fractional area per grid cell were provided by the species distribution model (LAVegMod.DM), resulting in a dynamic interaction between hydrodynamics and vegetation dynamics.

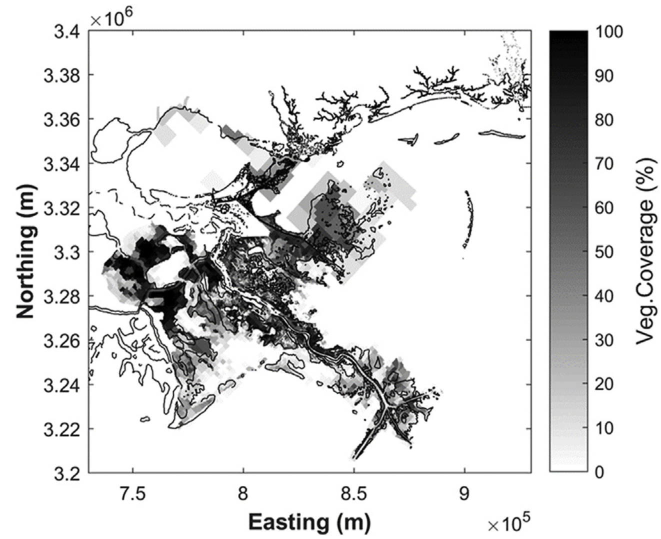

Fig. 3. Initial vegetation coverage map used in the model, based on the 2010 LULC dataset (Coastal Protection and Restoration Authority of Louisiana, 2012).

2.5. Morphodynamics component

The erosion and transport of fine sediment (silt, clay) is computed with the Partheniades erosion formulation (Ariathurai and Arulanandan, 1978) and the advection-diffusion equation (Lesser et al., 2004). These silt and clay fractions are easily erodible, with the clay fraction having a lower settling velocity and critical shear stress than the silt. Transport of sand as suspended load and bed load is computed with the van Rijn formulations (van Rijn, 2007a, 2007b).

A stratigraphy model was used to parameterize the subsoil of the morphodynamics component. Soil cores reveal that the surficial sediment layer (thickness of ∼1 m below NAVD88) was mostly organic marsh soil (Meselhe et al., 2015), with a critical shear stress for erosion of 1.5 Pa (no data available – based on expert judgment). At substrate depths greater than ∼1 m below NAVD88 in both Breton and Barataria receiving basins, coring data showed that sediment can be characterized as a consolidated clay. The material was assigned a critical erosion shear stress of 4 Pa to reflect this. Most of the open water in the receiving basins has a bed level of 1–1.5 m below NAVD88 and is therefore assigned the critical erosion shear stress of consolidated clay, assuming that the marsh layer had never formed there or had been removed by wave erosion during conversion from marsh to open water. This attribution was corroborated by selective coring in both basins of submerged areas. Sand content dominated the soil layers below the consolidated clay layer (10 m below NAVD88 and deeper; Stanley et al. (1996)). The bed composition in the Mississippi River channel was based on a calibrated and validated regional scale river model, designed based on field data (Allison et al., 2013).

Overall, five fractions were used in the morphodynamics component: (1) a marsh soil fraction representing the top wetland sediment layer, (2) consolidated clay representing the second wetland sediment layer, (3) fine clay (4) silt representing the suspended sediment load in the Mississippi River, and (5) coarse sediment (sand) representing the substrate and suspended sediment load in the Mississippi River. The morphological update was done at every computational time step (0.5 min in this model application) following Lesser et al. (2004). To reduce the simulation time, a morphological acceleration technique was applied where the bed update is scaled with a factor *MF* at every computational time step (Roelvink, 2006). The time scales associated with the hydrodynamics are typically two orders of magnitude shorter than with the morphodynamics resulting in *MF* values in the order of 1000 in relatively simple geometries, whereas lower values (~40) should be used in more complex geometries (Ranasinghe et al., 2010; van der Wegen et al., 2008).

2.6. Nutrient dynamics component

Biogeochemical and ecological processes relevant to the Louisiana coast but also to other coastal and deltaic systems (e.g., light attenuation, suspended sediment transport and deposition, as well as phytoplankton growth and mortality) were captured with the nutrient dynamics component (Fig. 1). The water quality processes in the nutrient dynamics component included various biogeochemical transformations via nitrogen, phosphorus, and carbon pathways and included interactions between the nutrients components, organic matter components, and the electron-acceptors in water and sediment/soil (Smits, 2013; Smits and van Beek, 2013).

The BLOOM model simulated phytoplankton growth and mortality (Smits, 2013). Given the wide range of salinities (0–20 ppt) in the Barataria and Breton estuaries, both freshwater phytoplankton (e.g., chlorophytes, diatoms, and cyanobacteria including the potentially toxic *Microcystis* spp. and *Anabaena* spp.) and marine phytoplankton (e.g., dinoflagellates) were modeled. Phytoplankton taxa and water quality constituents in the model are listed in Table 3.

Interactions at the sediment/soil-water interface were simulated using a "layered sediment" approach (Smits and van Beek, 2013), parameterizing the top 40 cm of the sediment/soil layer with seven sediment/soil depth layers. The upper layer was very thin (1 mm) and the bottom layer was thicker at 200 mm. The initial concentrations of constituents in the sediment/soil layers were defined using 2014 and 2015 field data (Meselhe et al., 2015).

The water constituents' loading was estimated based on discrete USGS water quality data from seven local rivers including the Mississippi River. The discrete data were used to construct rating curves between the water quality constituent concentrations and flow rates. Data were not available for all water quality constituents represented in the model. Thus, conversion relationships between water quality constituents with available rating curves were defined to estimate the loading of the remainder of the water quality constituents (Meselhe et al., 2015).

2.7. Vegetation dynamics component

The vegetation dynamics component simulates emergent vegetation biomass production, mortality, and allocation, as well as spatial distribution. The formulations of the vegetation dynamics model are described in detail in the Supplementary Materials (including Fig. SM1).

Seven emergent marsh vegetation taxa representing fresh, intermediate, brackish, and saline marsh types were selected to represent the wetland conditions (Table 3). The 2010 Land Use Land Cover (LULC) dataset from the 2012 Coastal Master Plan (Coastal Protection and Restoration Authority of Louisiana, 2012) was used to determine the initial vegetated spatial distribution. Fig. 3 shows the percentage vegetation coverage map for year 2010.

2.7.1. Vegetation biomass

The vegetation biomass model (VEGMOD) simulates the change in vegetation biomass and includes the effects of nutrient uptake, aboveground and belowground growth, and mortality of vegetation of seven key representative taxa (Table 3). The vegetation biomass model from Delft3D was extended with a formulation that incorporated 1) a seasonally varying biomass that accounts for the effect of nutrient availability on the total biomass, 2) the distribution of the biomass between the aboveground and belowground compartments using the vegetation biomass allocation model, 3) the incorporation of senescence (turnover) mortality and grazing-related mortality to the existing mortality related to inundation, and 4) the coupling of a vegetation species distribution model with the vegetation biomass model to consider spatial variation of vegetation coverage and taxa.

The existing vegetation biomass model calculates nutrient uptake and the pool of available nutrients (Smits, 2013). Nutrients (N, P and S) are taken up by vegetation from the sediment within the root zone (30 cm). The total uptake rates are computed using carbon to nutrient ratios (C:N, C:P, C:S) for specific taxa (Asaeda et al., 2002; Frost et al., 2009; Gessner, 2000; Ket et al., 2011; Laursen, 2004; Negrin et al., 2012; Osgood and Zieman, 1993; Qualls and Richardson, 2000; Richards and Ivey, 2004). For simplicity, the C:N, C:P and C:S values do not differ between the above- and belowground biomass for each taxa. The total uptake rates are distributed among the sediment layers within the rooting zone proportional to the quantities of the nutrients available in the layers.

Mortality decreases the vegetation biomass and transfers living vegetation to particulate detritus fractions. The mortality due to inundation was simulated as a first order decay process starting after water

Table 3
The list of phytoplankton and marsh vegetation taxa and water quality constituents simulated in the nutrient dynamics model. *1–4 indicates characteristics of organic matter simulated in the model; 1 means highly labile, and 4 means highly refractory.

Type	Model	Constituents
Nutrients	D-WAQ	Particulate organic carbon (POC1-4*), Dissolved organic carbon (DOC)
		Particulate organic nitrogen (PON1-4*), Dissolved organic nitrogen (DON), Ammonium (NH4), Nitrate (NO3),
		Particulate organic phosphorus (POP1-4*), Dissolved organic phosphorus (DOP), Phosphate (PO4), Absorbed phosphate (AAP), (Vivianite Phosphate (VIVP), Apatite phosphate (APATP),
		Particulate organic sulfur (POS1-4*), Dissolved organic sulfur (DOS), Sulfate (SO4), Dissolved Sulfide (SUD), Particulate Sulfide (SUP)
		Silicon (Si), Opal, Methane (CH4)
		Dissolved oxygen (DO), Silt, Clay, Sand
Phytoplankton	BLOOM	Freshwater diatoms (FDIATOMS), Freshwater flagellates (FFLGELA), Green algae (GREENS), *Microcystis* spp. (MICROSYSTIS), *Anabaena* spp. (ANABAENA)
		Marine diatoms (MDIATOM), Marine flagellates (MFLAGELA), dinoflagellates (DINOFLAG)
Vegetation	VEGMOD	*Typha* spp. (TYDO), *Phragmites* spp. (PHAU7), *Spartina alterniflora* (SPAL), *Spartina patens* (SPPA), *Sagittaria lancifolia* (SALA), *Sagittaria latifolia* (SALA2), *Zizaniopsis miliacea* (ZIMI)

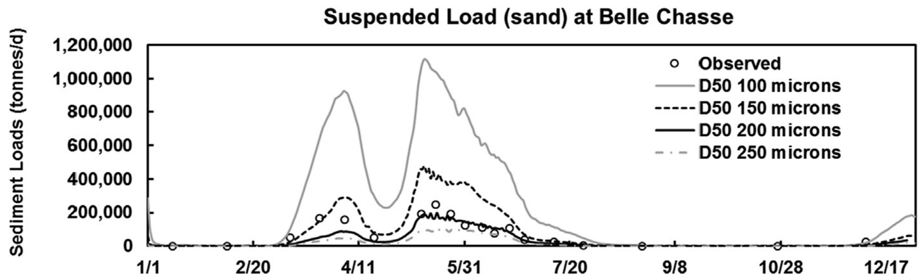

Fig. 4. Sensitivity analysis of the median diameter of coarse sediment (D50) model parameter compared to the field observations of sediment loads at Belle Chasse, Mississippi River in year 2011.

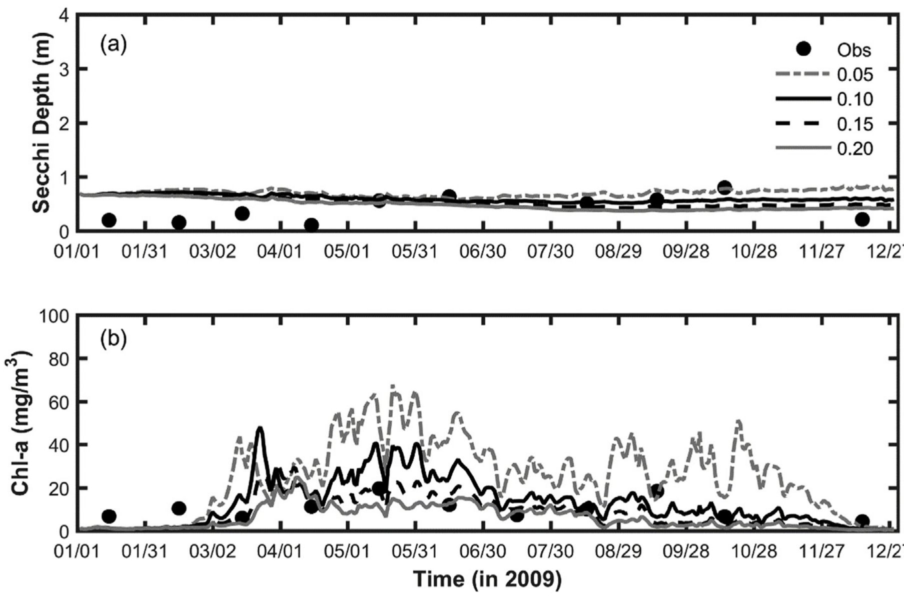

Fig. 5. Sensitivity test results using the fraction of DOC from POC (b_poc2doc). Change in b_poc2doc coefficients influences the (a) light penetration depth (Secchi disk depth) into water column and (b) changes of phytoplankton biomass (chl-a).

level has exceeded a critical depth and a critical duration (these thresholds varied by plant taxa). In the vegetation biomass model, detritus from the aboveground biomass is transferred to the water layers and detritus from the belowground biomass enters the sediment/soil layers. The detritus release rates are taxa dependent and are based on the C:N ratios of a taxa and the fraction of biomass allocated to a water or sediment/soil layer. This fraction was derived from vegetation height and rooting depth.

2.7.2. Species distribution of vegetation

The Louisiana Vegetation Model (LAVegMod), developed for Louisiana's 2012 Coastal Master Plan, was modified to provide the dynamics for seven taxa and integrate it with the other components of the Delft3D system (Visser and Duke-Sylvester, 2017; Visser et al., 2013). The establishment and mortality rates that vary with annual mean salinity and the annual standard deviation of water depth were estimated for each of the seven taxa (Meselhe et al., 2015) and the equations and general approach are described in detail in the Supplementary Materials (including Fig. SM2). An example of an establishment table for *Spartina alterniflora* is shown in Table SM1.

2.7.3. Vegetation biomass allocation

Plant root/shoot allocation is an important ecological process to determine how plants influence the hydrology and nitrogen cycling in wetland areas (Brouwer, 1962; Deegan et al., 2012; McConnaughay & Coleman, 1999). Overall, plants take up nutrients, their roots consolidate soils, and their stem density can influence flow velocities and trapping of sediment. The Integrated Biophysical Model presented here takes an evolutionary perspective for the vegetation biomass allocation model (LAVegMod.RootShoot) and assumes that allocating biomass to below-versus aboveground growth is a response that maximizes fitness over a range of nutrient concentrations (Hilbert, 1990; Johnson et al., 1985; Reynolds & Thornley, 1982; Thornley, 1972). When soil nitrogen is abundant, there is less demand to produce root biomass because existing root structures can obtain adequate quantities of nitrogen. The excess biomass is instead allocated aboveground to increase the capacity for photosynthesis. When soil nitrogen is scarce, there is an increased demand to allocate resources to root structures to obtain adequate nitrogen needed to sustain growth. The vegetation biomass allocation model was run concurrently with the other model components. The ratio is then used within the vegetation biomass allocation model to allocate the total vegetation biomass above- and belowground. The equations and general approach are described in detail in the Supplementary Materials.

3. Model performance assessment

Model sensitivity analysis was conducted via the perturbation and derivatives method (Pianosi et al., 2016). Model calibration and validation effort focused on the main stem of the river channel and the receiving basins. Observations from years 2009 and 2011 were utilized for the calibration and year 2014 for validation for most of the

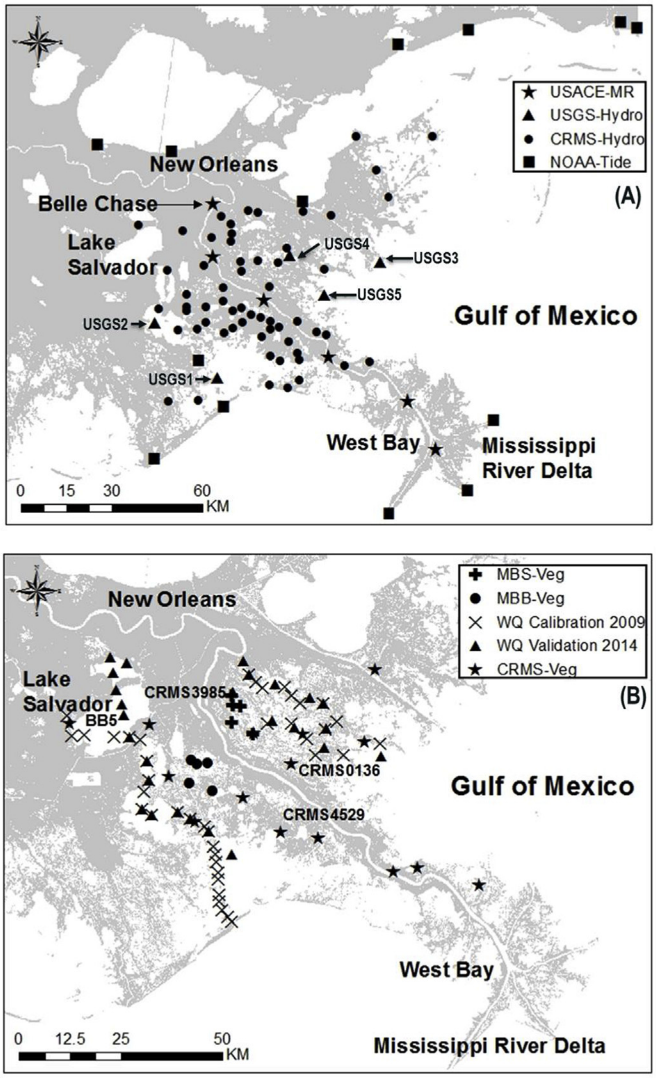

Fig. 6. Site locations for calibration and validation of the (A) hydro- and morphodynamics models and (B) nutrient and vegetation dynamics models. CRMS = Coastwide Reference Monitoring System, USACE = U.S. Army Corps of Engineers, USGS = U.S. Geological Survey and NOAA = National Oceanographic and Atmospheric Administration.

Table 4
Hydrodynamic model calibration coefficients.

Calibration Parameter	Areas	Ranges	Calibrated Values
Bed Roughness (Chezy)	Wetlands/Marshes	55–90	60
	Wetland Channels	65–110	75
	Shallow/Deep Water areas	65–90	75
	Mississippi River	60–120	63 to110
Horizontal Eddy Diffusivity	Inner domain with fine grid (Wetlands)	1–10	10
	Outer domain with coarse grid (GOM)	50–200	150
	Transition between Inner and Outer domain	N/A	Linear Interpolation

components. Year 2011 was a wet year in the Mississippi River Basin with record levels of precipitation resulting in record river stage and flow conditions. Years 2009 and 2014 were more typical of average flow conditions in the Mississippi River.

3.1. Sensitivity analyses

The open water diffusion controls the hydrodynamics in the model. Delft3D calculates diffusion at the scale of the grid cell. To resolve significant mixing that may occur at the sub-grid spatial scale, Delft3D employs a diffusion coefficient parameter that adds a constant mixing rate to that already calculated to occur at the grid cell scale. Furthermore, for depth-averaged simulations, the diffusion coefficient should also incorporate the dispersion effect caused by vertical flow shear. Hence, the diffusion coefficient is one of the important parameters to adjust during the calibration phase of the hydrodynamics component. For sensitivity tests, four diffusion coefficient setups were considered: (1) uniform value equal to 1 $m^2 s^{-1}$ in the entire domain; (2) calibrated spatially variable diffusion coefficient; (3) the calibrated spatially variable distribution multiply by 10 (one order of magnitude greater); (4) calibrated spatially variable distribution divided by 10 (one order of magnitude lower). Hydrodynamic model runs occurred for one year (2010), for existing conditions and for existing conditions with a riverine point source (from Mississippi River into the mid-Barataria Basin area). Model results indicate that the saline water barely penetrates into Barataria Bay when the diffusion coefficient is low (uniform 1 or one order of magnitude lower). In contrast, too much saline water enters Barataria Bay when the diffusion coefficient was high (one order of magnitude greater) (see Supplementary Materials, Figs. SM2 and SM3). The perturbation and derivation method of sensitivity analysis was used to finally select the calibrated spatial distribution of diffusion coefficient for the model.

Sensitivity analysis was also performed on the morphodynamic model. The median diameter of coarse sediment (D50) values of 100, 150, 200 and 250 μm was perturbed one at a time. The impacts on the simulations were assessed via visual inspection by comparing the time series of total sand transport in the Mississippi River near Belle Chasse (Fig. 4). D50 of 200 μm was selected for providing the best agreement with the field data.

Variation of the model output from the nutrient dynamics component was investigated to better understand how light penetration and phytoplankton biomass (chl-a) are influenced by an uncertain model parameter of dissolved organic carbon (DOC) that is mathematically derived from particulate organic carbon (POC). The parameter (b_poc2doc) was adjusted and compared to field observations from year 2009 to investigate the model output sensitivity (Fig. 5). The value of 0.10 was selected for b_poc2doc because it closely aligned with the field data.

3.2. Calibration and validation

The field measurement locations used to calibrate and validate the Integrated Biophysical Model are shown in Fig. 6. Manual tuning was preferred over automatic calibration because of the complexity of the coupled models which resulted in time constraints and computational demands. Our integrated model requires 24–48 h to complete a single year run. Attempting to use an automated calibration approach with such long run times was not possible given the time constraints placed on model development and deployment to support management decisions. Automated calibration algorithms trade the need for deep expertise with a model and its application for a degree of computationally expensive approach in the search for optima. Automated calibration algorithms can also spend time exploring local optima before finding better parameter combinations. In many instances, the computationally expensive approach of an automated search is acceptable. However, the long run time of our model makes that approach involved in automated algorithms impractical. Instead, we applied our own expertise with the model and the ecosystem to guide the calibration process towards appropriate parameter values in a more efficient manner.

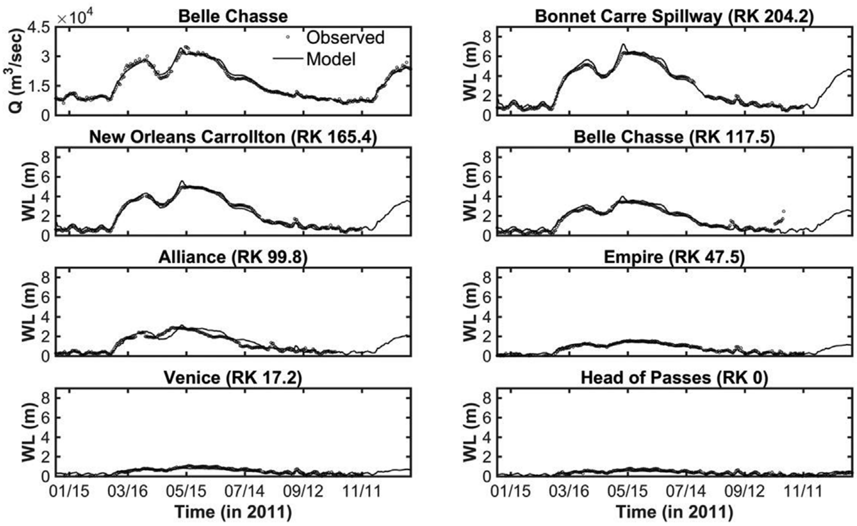

Fig. 7. Comparison between model results (flow and water level) and field measurements in the Mississippi River.

Table 5
Model performance assessment for calibration of water levels within the Mississippi River channel.

Station	Average Bias (m)	Bias % of Range	RMSE (m)	RMSE (%)	Correlation Coefficient (r)
Bonnet Carré	0.08	0.45	0.28	1.59	0.99
New Orleans - Carrollton	−0.01	−0.03	0.22	0.70	0.98
Belle Chasse	0.04	+0.15	0.23	0.81	0.98
Alliance	−0.08	−0.26	0.17	0.60	0.98
W Point a La Hache	0.05	+0.20	0.22	0.89	0.96
Empire	0.03	+0.09	0.17	0.59	0.96
Venice	0.04	+0.22	0.22	1.34	0.95
Head of Passes	0.05	+0.51	0.19	1.91	0.84

Table 6
Observed and modeled flow results (calibration) in the Mississippi River Delta tributaries (year 2011).

Upstream Flow (m^3/s)	Station	Model Flow (m^3/s)	Rating Curve (m^3/s)	Bias (%)
31,150	Bohemia and Fort St. Philip and Ostrica (Overbank losses)	3898	4201	−7.2
	Baptiste Collette	3019	2944	2.5
	Grand Pass & Tiger Pass	2572	2876	−10.6
	West Bay	1521	1907	−20.3
	Cubit's Gap	3593	3406	5.5
	SW Pass	8258	10,775	−23.4
	South Pass	2771	2649	4.6
	Pass-A-Loutre	2024	2079	−2.7
21,800	Bohemia and Fort St. Philip and Ostrica (Overbank losses)	2217	2097	5.7
	Baptiste Collette	2313	2126	8.8
	Grand Pass & Tiger Pass	1859	2150	−13.5
	West Bay	1420	1389	2.2
	Cubit's Gap	2534	2360	7.4
	SW Pass	7178	7453	−3.7
	South Pass	2390	1968	21.4
	Pass-A-Loutre	1733	1649	5.1
14,150	Bohemia and Fort St. Philip and Ostrica (Overbank losses)	1005	808	24.4
	Baptiste Collette	1439	1454	−1.1
	Grand Pass & Tiger Pass	1127	1553	−27.4
	West Bay	1029	965	6.6
	Cubit's Gap	1624	1500	8.3
	SW Pass	4984	4721	5.6
	South Pass	1864	1415	31.7
	Pass-A-Loutre	1347	998	34.9

3.2.1. *Hydrodynamic component*

The hydrodynamics component was calibrated against 40 stations measuring salinity, water level, temperature, and velocity. The calibration parameters were adjusted by sensitivity analysis until the model results showed reasonable agreement with the data. The bed roughness (Chezy value) was the main parameter used in the hydrodynamic calibration-validation process, and was iteratively adjusted until the simulated and observed data achieved a reasonable agreement. The sensitivity of horizontal eddy diffusivity was also tested between the inner domains of the basins and the Gulf of Mexico. The parameters (and their ranges) used for sensitivity test are listed in Table 4. A sample of the model performance evaluations are shown here – further details can be found in Meselhe et al. (2015). For the Mississippi River channel, the model output of flow and water level were compared to field measurements and fit statistics were performed (Meselhe and Rodrigue, 2013). The model results were well correlated with the observed water levels with correlation coefficients ranging between 0.84 and 0.99 (Fig. 7, Tables 5 and 6 - see Meselhe et al., 2015 for further details) and fit statistics were performed (Meselhe and Rodrigue, 2013). In addition, comparisons were made for the flow distribution at various overbank and tributaries of the Mississippi River Delta (Table 6 against the rating curve data developed from previous studies (Allison et al., 2012).

Comparison of observed and modeled tidal constituents for years 2009 and 2011 were conducted with 12 NOAA stations located in the model domain. Harmonic analysis was performed on the time series of simulated water level to extract amplitude and phase of four tidal constituents: principal lunar semidiurnal cycle (M2), the principal solar semidiurnal cycle (S2), the combined lunar and solar semidiurnal cycle (K1), and lunar diurnal constituent (O1) (https://tidesandcurrents.noaa.gov/glossary.html#M), which are the dominating tides at these stations (approximately 50% of total tidal amplitude). Overall, the model predicted the tidal amplitudes and phases well with the difference between the modeled and observed in tidal amplitude ranging between −0.3 cm and 1.4 cm and the difference in the phase ranging between 12.3 and 1.0° (Table 7- see Meselhe et al., 2015 for further details). The model also captured the overall trend and reproduced the low-frequency water level fluctuation resulting from storms and river floods at most of the stations in both basins for the years of 2009 and

Table 7
Model calibration for 12 NOAA stations in the computed harmonic constituents for the years 2009 and 2011.

	M2 amp (cm)	M2 phase (deg.)	S2 amp (cm)	S2 phase (deg.)	K1 amp (cm)	K1 phase (deg.)	O1 amp (cm)	O1 phase (deg.)
2009 Mean Error	−0.3	−1.6	−0.2	−11.2	0.7	1.0	1.4	−0.6
2011 Mean Error	−0.2	−2.4	−0.2	−12.3	0.0	−1.2	0.3	−1.2

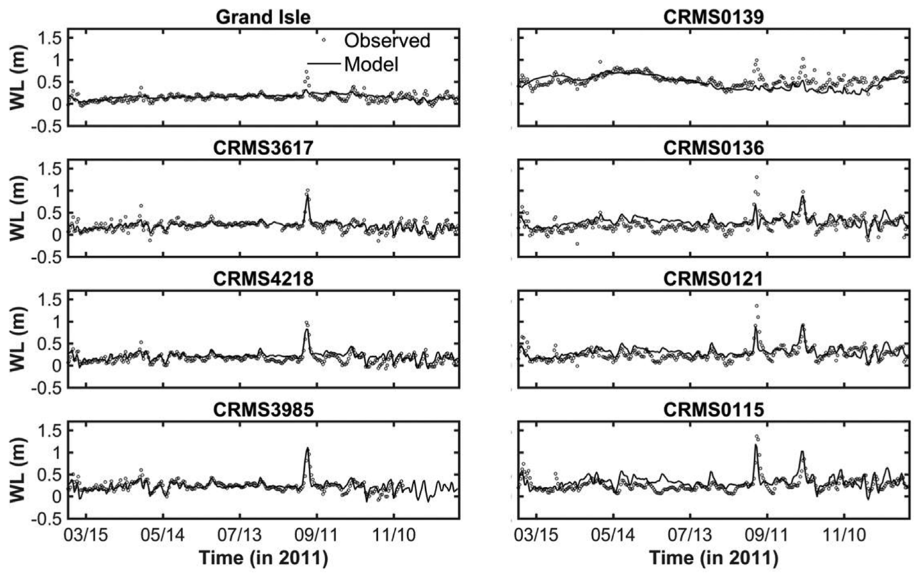

Fig. 8. Comparison between the calibrated model-derived and observed water levels in Barataria Basin at Grand Isle, CRMS3617, CRMS4218, and CRMS3985, and in Breton Basin at CRMS139, CRMS136, CRMS121 and CRMS115.

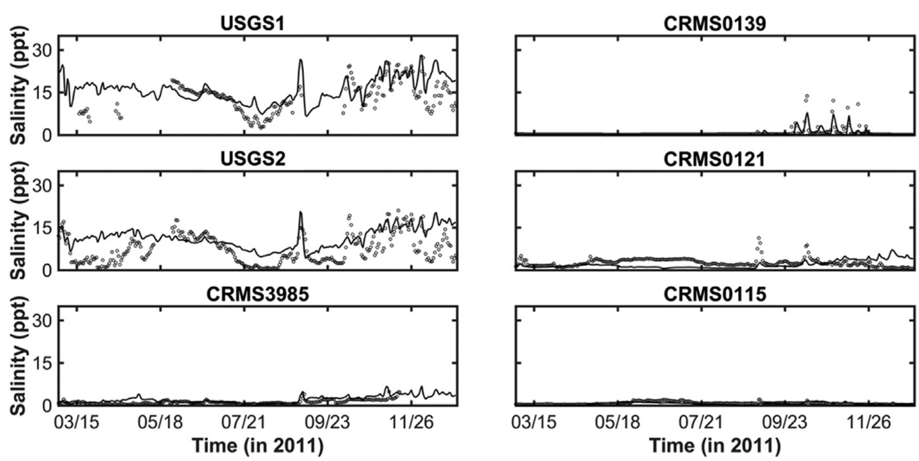

Fig. 9. Comparison between the model-derived depth averaged and the observed surface water salinity in Barataria Basin at USGS1, USGS2, CRMS3985, and in Breton Basin at CRMS139, CRMS121, CRMS115.

2011 (see Meselhe et al., 2015 for further details). Fig. 8 demonstrates an example of the model derived water level comparison against field observations.

The computed salinity increases from the upper basin to the lower basin in both Barataria and Breton basins, were in agreement with observed data for 2009, 2011, and 2014 (Meselhe et al., 2015). The reproduction of the horizontal salinity gradients suggests that the model captured the horizontal mixing of fresh and salt water. An example of model results comparison is shown in Fig. 9. Visual inspection of the comparisons and assessment via performance statistics demonstrate that the modeled salinity values correspond reasonably well to observations for most of the stations (Table 8).

Water temperature calibration and validation in the Barataria and Breton basins were performed by comparing the model results to USGS observed data in year 2009, 2011, and 2014 (Meselhe et al., 2015). The model represented well the seasonal change in water temperature in this system (Fig. 10, Table 9).

3.2.2. Morphodynamics component

The sediment transport and morphology model was calibrated (2011) and validated (2014) with observational data in both riverine and coastal environments. The governing processes for sediment dynamics within the Mississippi River channel are different from those in the receiving basins. For example, fine sediments are easily transported and vertically well mixed in the Mississippi River because of the high-energy and unidirectional flow. Conversely, fine particles are more likely to deposit in low-energy areas of the receiving basins, especially where vegetation exists. Calibration parameters for fine sediment

Table 8
Model performance assessment for salinity in the Barataria and Breton basins for calibration (Year 2011, 2009) and validation (Year 2014).

Year	Station	Mean (Measured) (ppt)	Mean Bias (ppt)	Mean Corr. Coef. (r)	RMSE (ppt)
2011	USGS1	13.42	3.05	0.58	5.29
	USGS2	5.91	3.97	0.52	5.75
	CRMS3985	1.16	0.63	0.72	0.98
	CRMS139	0.61	−0.19	0.86	0.58
	CRMS121	2.58	−0.66	0.34	2.19
	CRMS115	0.74	−0.17	0.57	0.42
2009	USGS1	8.70	0.63	0.61	3.48
	USGS2	3.43	0.43	0.49	2.57
	CRMS3985	N/A	N/A	N/A	N/A
	CRMS139	0.25	−0.22	0.50	0.29
	CRMS121	2.50	−0.92	0.94	1.26
	CRMS115	0.54	−0.03	0.94	0.35
2014	USGS1	11.53	6.74	0.77	7.64
	USGS2	6.41	7.48	0.68	8.23
	CRMS3985	1.18	3.38	0.40	3.63
	CRMS139	0.38	−0.07	0.47	0.63
	CRMS121	3.65	0.72	0.80	2.15
	CRMS115	1.57	1.50	0.95	2.24

includes: critical shear stress (Tcr), sediment erosion rate (M) and settling velocity (Vs). Settling velocity and the critical shear stress are the main calibration parameters adjusted in the calibration and validation process. Table 10 presents a summary of the calibrations parameters for fine sediment with their ranges used in sensitivity tests. The computed sediment load was compared to the River's measured load (see Fig. 11). The computed amount of sediment deposited in an existing non-controlled sediment diversion (West Bay, see Fig. 6 for location) was compared to observations. The computed annual sediment deposition corresponds well with observations (Fig. 12). The discrepancy in the distribution of deposited sediment likely results from wave resuspension which is not represented in this Integrated Biophysical Model.

3.2.3. Nutrient dynamics component

The nutrient dynamics are driven by the flow field, salinity, and temperature computed in the hydrodynamic model. Through a direct link with the vegetation biomass model, the nutrient dynamics component also simulates the biogeochemical processes for each constituent (see Table 3) in both the water column and the sediment/soil layers.

The nutrient dynamics component was calibrated and validated by tuning and compared against observations in both basins for years 2009 (calibration) and 2014 (validation). Model performance was evaluated by graphical comparison between modeled and observed data and statistical analysis (i.e., bias, RMSE, and correlation coefficient). Initial coefficient values were derived either from the literature or previous studies, e.g., Smits and van Beek, (2013); Los (2009). The model calibration parameter values are summarized in Table 11. Fit statistics were calculated to help assess water quality model performance (Los and Blaas, 2010). The model results as shown in Table 12 and Fig. 13 demonstrate that many of the model parameters agree well with the observations (for further details see Meselhe et al., 2015). Certain parameters, such as Chl-a, NH4, TSS, TP, and PO4 need to be improved in future modeling tasks. In addition, the confidence in the statistical assessment (see Table 12) of the model performance proves challenging when the sample size of observations are insufficient or small.

Table 9
Statistical summary of water temperature calibration (2009 and 2011) and validation (2014).

Time period	Location	Bias (°C)	Corr Coeff (r)	RMSE (°C)
2009	USGS2	0.4	0.98	1.1
	USGS4	−1.1	0.96	1.6
2011	USGS1	0.2	0.96	1.3
	USGS5	−0.8	0.97	1.4
2014	USGS1	0.1	0.96	1.8
	USGS2	0.3	0.96	1.7
	USGS3	−0.6	0.97	1.7
	USGS4	−1.11	0.94	2.1

Phytoplankton composition of the main phytoplankton groups was compared to summer observational data (June and August, 2014) (data not shown). Two most common groups of phytoplankton during August were diatoms and chlorophytes and the model tended to reasonably capture these conditions in Barataria Basin. However, the model showed some limitation to determine the dominant phytoplankton groups during June and August in Breton Basin. Discrepancies between modeled and observed results may be due to the limited local understanding of critical parameters for different phytoplankton groups, such as growth rates, optimum temperature, mortality rates at various salinities, etc.

3.2.4. Vegetation dynamics component

The vegetation biomass model simulates plant biomass dynamics for each of the seven taxa used in the model. Unfortunately, there was no observed data for vegetation biomass in 2009 and 2011. Vegetation data collected during 2014 (Meselhe et al., 2015) were used as a

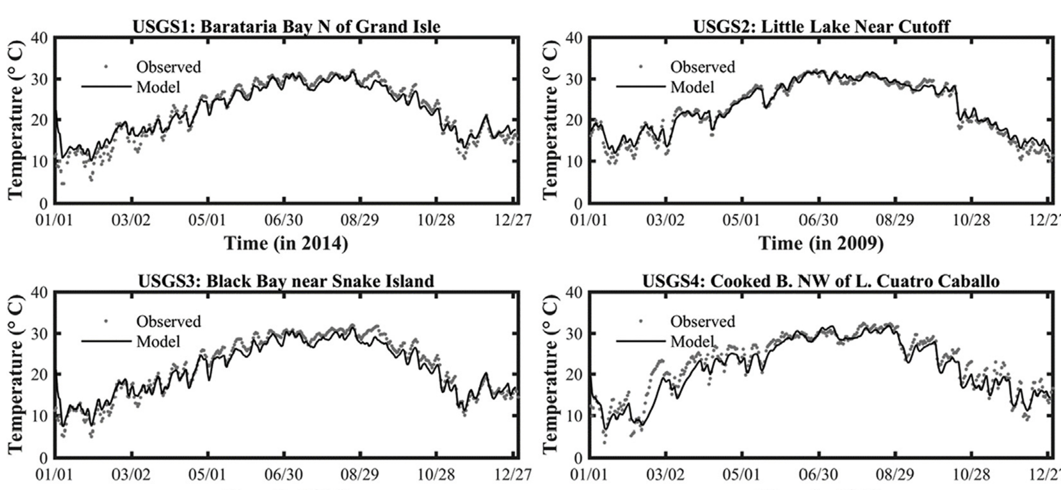

Fig. 10. Comparison between the model-derived depth averaged and the observed surface water temperature in Barataria Basin at USGS1 and USGS2, and in Breton Basin at USGS3 and USGS4.

Table 10
Morphodynamics component calibration coefficients.

Calibration Parameters	Ranges	Calibrated Values			
		Silt	Clay	Marsh Soil	Consolidated Clay
Settling Velocity (mm/sec)	1–0.001	0.1	0.001	0.1	0.1
Critical Shear Stress (Pa)	0.01–5	0.15	0.01	1.5	4.0
Sediment Erosion Rate (kgm^{-2}s^{-1})	0.0001–0.001	0.001	0.001	0.001	0.001

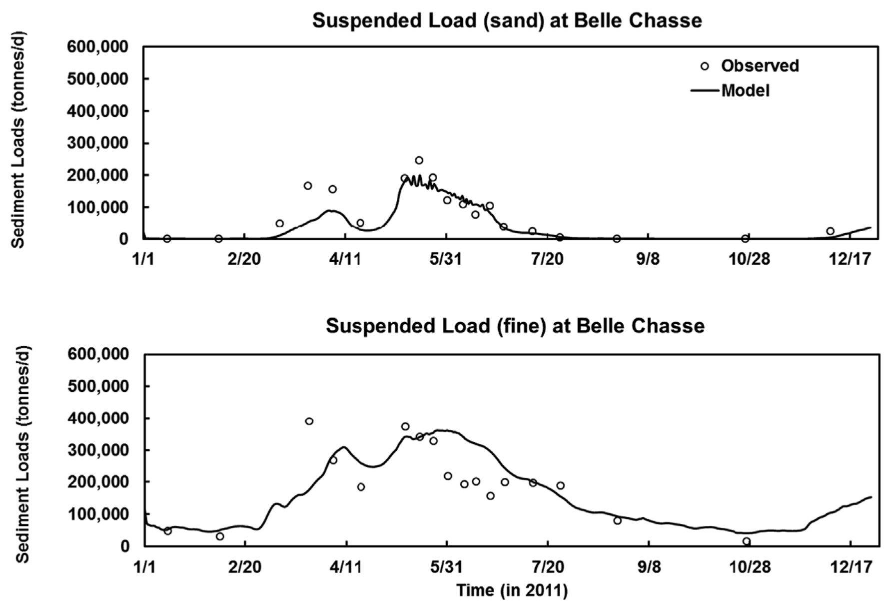

Fig. 11. Computed and observed sand load (top) and clay + silt load (below) at Belle Chasse.

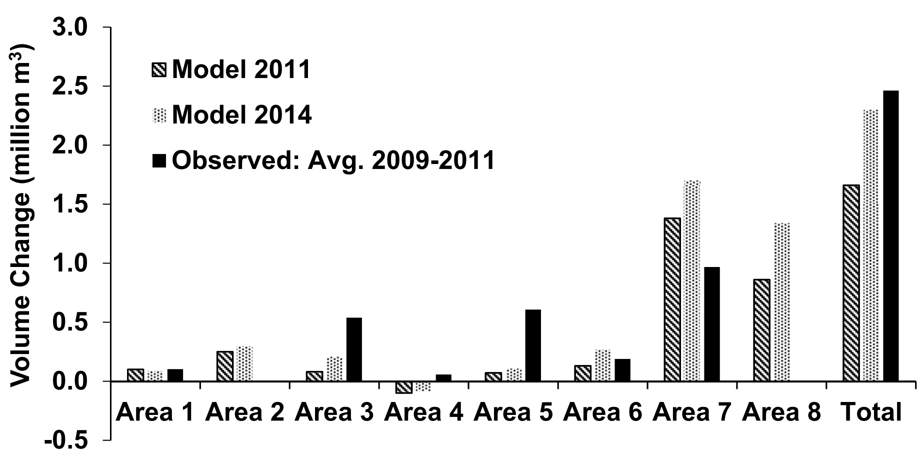

Fig. 12. Computed (2011, 2014) and observed (2009–2011) sediment deposition from the Mississippi River.

reference with an assumption that seasonal vegetation biomass changes observed in 2014 are similar to those for 2009 and 2011. Aboveground vegetation biomass data were collected at 24 sites (15 CRMS, 5 MBB, and 5 MBS sites) in 2014 (see map in Fig. 6) in Barataria and Breton basins and were compared to model results (Meselhe et al., 2015). The vegetation total maximum biomass curves (Fig. 14), vegetation growth, and mortality rates for each vegetation taxa were used to calibrate the aboveground vegetation biomass dynamics. Table 13 lists the coefficients from model calibration.

Vegetation biomass values were compared to observed data collected in 2014 at 24 sites (Table 14). Both observed and simulated biomass values were converted to g C m^{-2}. The correspondence between the model and observed biomass was mixed for site CRMS0136 (Fig. 15a), which was in Breton Basin (see Fig. 6). Observed data indicated that most of the biomass is represented by SPPA (327 g C m − 2), with a smaller contribution from SPAL (53 g C m − 2) and from non-modeled species (49 g C m − 2). Like observed results, the model predicts a large contribution from SPPA (191 g C m − 2). However, the second tier of biomass contribution predicted by the model is different from observed data (Fig. 15a).Fig. 15b shows a comparison for site 4529 (see Fig. 6), which is in the lower Barataria Basin. The model results at this location correspond well to the observed biomass values.

Table 11
Nutrient dynamics model calibration coefficients.

Processes	Coefficients		Ranges	Calibrated Values Water		Sediment/Soil	
				Veg	Unveg	Veg	Unveg
Phytoplankton	Mort2MIC	Mortality at chloride = 0 for MICROCYSTIS (1/day)	0.035–0.08	0.08	0.08	–	–
	Mort2ANA	Mortality at chloride = 0 for ANABAENA (1/day)	0.035–0.08	0.08	0.08	–	–
	V0SedFFL	Sedimentation rate for FFLAGELA (m/day)	0.0–1.5	0.25	0.25	–	–
	V0SedGRE	Sedimentation rate for GREENS (m/day)	0.0–1.5	0.5	0.5	–	–
	V0SedMIC	Sedimentation rate for MICROCYSTIS (m/day)	0.0–1.5	0.5	0.5	–	–
	V0SedANA	Sedimentation rate for ANABAENA (m/day)	0.0–1.5	0.5	0.5	–	–
	V0SedMDI	Sedimentation rate for MDIATOMS (m/day)	0.0–1.5	0.5	0.5	–	–
	V0SedMFL	Sedimentation rate for MFLAGELA (m/day)	0.0–1.5	0.25	0.25	–	–
	V0SedDIN	Sedimentation rate for DIOFLAG (m/day)	0.0–1.5	0.25	0.25	–	–
Organic Matter	b_poc2doc	Fraction POC2 converted to DOC (−)	0.05–0.2	0.10	0.10	0.10	0.10
	b_poc3doc	Fraction POC3 converted to DOC (−)	0.05–0.2	0.10	0.10	0.10	0.10
Electron acceptors	KsNiDen	Half saturation constant for NO3 limitation (gN/m^3)	0.05–0.4	0.25	0.25	1.0	0.25
	CoxDenInh	Critical diss. ox. Conc. for inhib. denitrifi. (g/m^3)	1.0–10.0	1.0	1.0	10.0	10.0
	KsOxDenInh	Half saturation constant for oxygen inhibition (g/m^3)	0.1–2.0	2.0	2.0	1.0	2.0
Inorganic N	KsAmNit	Half saturation constant for NH4 limitation (gN/m^3)	0.1–0.7	0.2	0.2	0.2	0.2
	KsOxNit	Half saturation constant for DO inhibition (g/m^3)	0.05–1.0	0.5	0.5	0.5	0.5
	RcNit20	MM-nitrification rate at 20 °C ($gN/m^3/d$)	0.1–30	0.2	0.2	30.0	30.0
Inorganic P	fr_FeIM1	Fraction Fe in inorganic matter IM1 (−)	0.025–0.075	0.034	0.034	0.034	0.034
	fr_FeIM2	Fraction Fe in inorganic matter IM2 (−)	0.025–0.075	0.034	0.034	0.034	0.034
	fr_FeIM3	Fraction Fe in inorganic matter IM3 (−)	0.0	0	0	0	0
	fr_Feox	Fraction reactive Fe of total Fe (−)	0.1–1.5	0.5	0.5	1.5	1.5
	KadsP_20	Absorption equilibrium constants at 20 °C	1000–3000	1200	1200	1200	1200
	RatAPandVP	Ratio of apat. and vivian. Precipitation rate (−)	0.0–2.0	0.0	0.0	0.0	0.0
	EqAPATDisp	Equilibrium conc. PO4 with apatite (gP/m^3)	0.05–0.25	0.1	0.1	0.1	0.1
Settling, other than phytoplankton	V0SedPOC	Settling velocity for POC 1 to 4 (m/day)	0.0–1.0	1.0	0.5	–	–
	V0SedIM1	Settling velocity for silt (m/day)	0.0–1.0	0.15	0.025	–	–
	V0SedIM2	Settling velocity for clay (m/day)	0.0–1.0	0.05	0.005	–	–
	V0SedIM3	Settling velocity for sand (m/day)	0.0–1.0	3.0	3.0	–	–

Table 12
Average error estimates for water quality variables in the Barataria and Breton basins.

Year	Basin	WQ Variable	Mean	Bias	Unbiased RMSD
2009	Barataria (25 stations)	Chl-a (ug/l)	15.87	−4.70	15.01
		TN (mg/l)	0.79	0.18	0.33
		NH4 (mg/l)	0.02	−0.02	0.03
		NO3 (mg/l)	0.24	0.19	0.16
		TP (mg/l)	0.13	0.08	0.03
		PO4 (mg/l)	0.08	0.03	0.03
		SiO2 (mg/l)	1.86	0.00	1.09
		TSS (mg/l)	15.19	−24.20	47.75
	Breton (15 stations)	Chl-a (ug/l)	35.59	15.93	33.44
		TN (mg/l)	1.06	0.20	0.36
		NH4 (mg/l)	0.03	−0.02	0.04
		NO3 (mg/l)	0.30	−0.07	0.38
		TP (mg/l)	0.12	0.02	0.05
		PO4 (mg/l)	0.06	0.01	0.07
		SiO2 (mg/l)	1.82	0.02	1.04
		TSS (mg/l)	25.48	−9.40	37.65

The observed biomass totaled 375 g C m^{-2} and was all invested in a single species, *S. alterniflora* (SPAL). The vegetation models predicted a total biomass of 269 g C m^{-2} at this location, with most of the biomass being invested in SPAL. Three other taxa, *Phragmites* spp. (PHAU7), *S. patens* (SPPA), and *S. lancifolia* (SALA), were also predicted to be present, but they made relatively small contribution to the overall biomass. See Meselhe et al. (2015) for vegetation biomass comparison results for seven vegetation taxa at CRMS sites. In addition, more information about the discrepancies can be found in section 4.0 Discussion.

3.3. Coupled hydrodynamics, nutrient dynamics, and vegetation dynamics components

The vegetation dynamics component (biomass and species distribution) was influenced by the hydrodynamics component through the effects of inundation related stressors to the marsh vegetation biomass as well as the niche characteristics (salinity and water level) of the vegetation taxa. The vegetation height of each of the taxa (simulated in biomass model) dictates when a critical prescribed threshold of water depth was reached which results in the addition of an inundation mortality rate. These processes influence the biomass production of the vegetation (Fig. 16a).

The feedbacks between the nutrient dynamics and vegetation dynamics component (biomass and species distribution) are incorporated into the model because of the importance of soil porewater nutrients to the growth of vegetation biomass and the effects plant nutrient uptake has on the availability of nutrients for other organisms, such as phytoplankton. In Fig. 16b, during the growing season, marsh vegetation (*Spartina patens*) removes ammonium from the soil porewater and builds aboveground biomass resulting in a depletion of ammonium concentrations. This results in an increase in the flux of particulate organic carbon to the top soil layers (Fig. 16c). Once the vegetation biomass starts to senesce during the fall season, the ammonium porewater concentrations return via organic matter remineralization (Fig. 16b and c).

3.4. Coupled hydrodynamics, morphodynamics and vegetation dynamics components

As mentioned previously, there is a strong bidirectional interaction between vegetation and hydrodynamics. To demonstrate the influence of vegetation on the flow field and morphology, a model experiment was performed with and without vegetation. Fig. 17 shows the difference in the bed elevation in the simulation experiments with and without vegetation, where the areas identified in cold colors reflect the additional sediment deposition due to the presence of vegetation. The sediment deposited in the simulation experiment with vegetation would have been transported further out by the flow – hence the hot colored areas shown in Fig. 17.

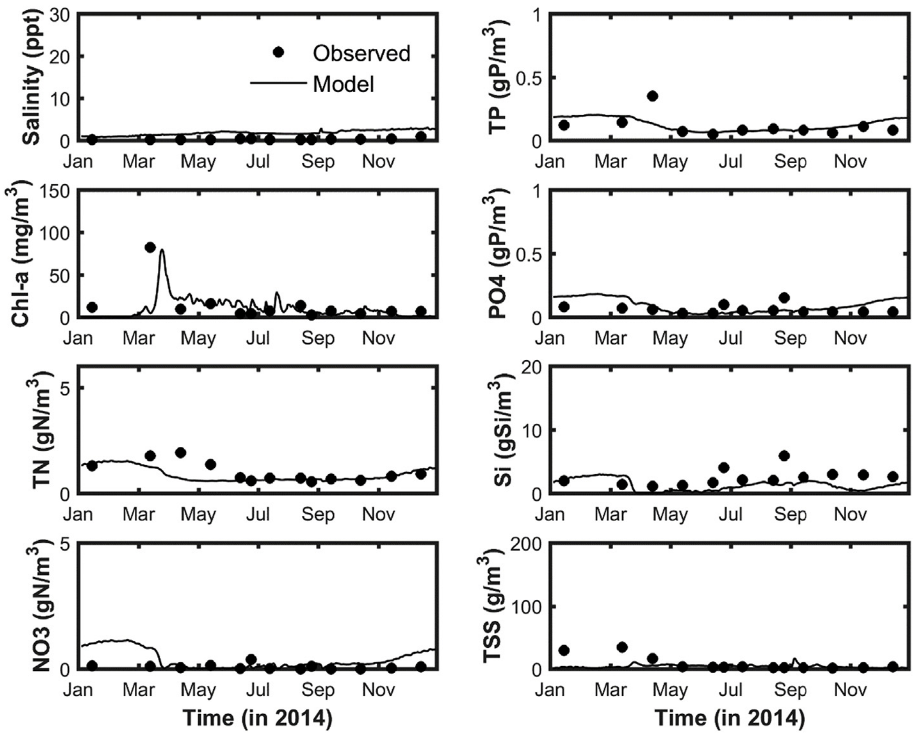

Fig. 13. Example of water quality model comparison results at Lake Salvador (BB5) in Barataria Basin, west of the Mississippi River.

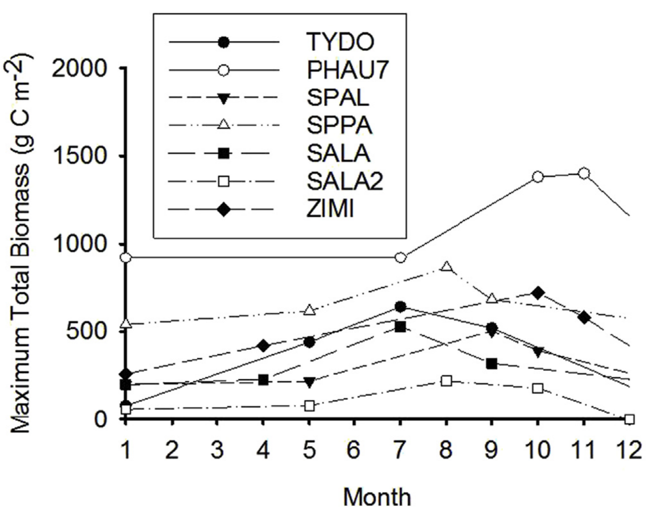

Fig. 14. The maximum (or target) total biomass (aboveground + belowground) curves of seven vegetation taxa. See Table 3 for scientific name.

4. Discussion

Human and natural impacts on estuarine ecosystems can be quantified with various models including the effects of hydrodynamics, nutrient dynamics, vegetation dynamics, and morphodynamics. Such models typically focus on one or few aspects (hydrodynamics, morphodynamics or vegetation dynamics) while oversimplifying or omitting the others (Wolanski and Elliot, 2015). The integrated model presented here is a significant advancement in modeling deltaic and coastal systems because (a) it captures the interaction and feedback among various hydrologic, morphologic, and ecological processes; and (b) it is applicable to large spatial ecosystems and at a long temporal scale (decadal). The benefits of using on-line (two-way) feedback include better representation of the natural environments because of the dynamic interactions. However, the limitations of this approach include a computationally heavy model that requires an interdisciplinary team to interact with and interpret its results.

4.1. Hydrodynamics and morphodynamics components

The water levels, discharges, velocities, and salinities at various sites along the lower Mississippi River and the receiving basins were well captured. Further, the sediment loads at Belle Chasse (see Fig. 11) within the Mississippi River channel and deposition patterns at the outfall area of the West Bay sediment diversion (see Fig. 6 for the location of these stations and areas) also compared well against the available information in the literature or field measurements. The model performance has been assessed in a quantitative manner using statistical tools defined in Meselhe et al. (2015). The model results captured the flow distribution through the passes reasonably well. Table 5 shows the model results and how they compare to data-based rating curves. In the upper and middle basins, the modeled salinities compared well against the observations in the upper and middle of the basins but not as well in the lower portion of the basins. This could be attributed to possible salinity stratification that would not be captured with this depth-averaged model (2D), and due to the scarcity of available open water measurements of salinity, there are uncertainties related to the prescribed boundary conditions assigned. Currently, the model includes the influence of wind-driven resuspension and tidal circulation and how they redistribute sediment in the receiving basins. Future model versions should consider assessing the role of waves and weather events (e.g. winter storms also known as cold fronts) on redistribution of sediment in coastal areas and erosion of wetlands. The model architecture allows a full coupling with the SWAN wave model, but at this stage has not yet been included. The impacts of storms, including pressure and waves should be considered in future versions of this model because these events can have substantial effects on the wetland vegetation, distribution of deposited sediment, and morphological features. Including the physical destruction of storms on vegetated habitats would require a higher frequency of coupling (less than annual) to incorporate these potential drivers.

Table 13
Vegetation growth and mortality rates of seven taxa used in vegetation biomass model. See Table 3 for scientific name.

Parameter	Description	TYDO	PHAU7	SPAL	SPPA	SALA	SALA2	ZIMI	Source
Rc0GWV	net growth rate at 20 °C (1/d)	0.1	0.1	0.1	0.1	0.1	0.1	0.1	Duke-Sylvester and Visser personal communication
TcGWV	temperature coefficient of growth (−)	1.072	1.04	1.04	1.072	1.04	1.04	1.04	Asaeda and Karunaratne, 2000; Soetaert et al., 2004
Rc0MSWV	senescence mortality rate at 20 °C (1/d)	0.025	0.025	0.0075	0.0125	0.0125	0.0125	0.0125	Asaeda and Karunaratne, 2000; Best et al., 2011; Soetaert et al., 2004
TcMSWV	temperature coefficient of senescence mortality	1.07	1.07	1.07	1.07	1.07	1.07	1.07	Deltares and WI assumptions
CrdepVB	critical depth (m) for inundation mortality	0.75	0.70	0.2	0.21	0.30	0.34	0.50	Birch and Cooley, 1982; Stutzenbaker, 2010
VegHeVB	vegetation height (m)	2.5	3.5	1.0	1.03	1.2	1.35	1.65	Adams and Bate, 1999; Asaeda and Karunaratne, 2000; Bertness, 1991, 1985; Birch and Cooley, 1982; DeLaune et al., 1979; Fox and Haller, 2000; Frost et al., 2009; Gerard, 1999; Grace, 1989; Gross et al., 1991; Hester et al., 1996; Hogg and Wein, 1988; Howard and Mendelssohn, 1999; Johnson et al., 1985; Ket et al., 2011; Lorenzen et al., 2001; Mendelssohn et al., 1981; Richards and Ivey, 2004; Stanton, 2005; Stutzenbaker, 2010; Weisner and Miao, 2004
CNF2VB	carbon nitrogen ratio (aboveground)	48.2	35	71.2	108	28.5	32.4	50.2	Vegetation biomass allocation model
CPF2VB	carbon phosphorus ratio (aboveground)	1266	1700	1758	2371	614	27.2	1079	Vegetation biomass allocation model
RcMrtVB	inundation mortality rate (1/d)	0.0	0.0	0.0	0.0	0.0	0.0	0.0	Expert assumptions
CrnsfVB	lag time (day) for inundation mortality	1	1	1	1	1	1	1	Expert assumptions

4.2. Nutrient dynamic component

The nutrient dynamics component captured the general temporal and spatial nutrient dynamics, and the model compared well against most of the field observations. Including the sediment/soil layers in the model helped to represent the important nutrient fluxes between the sediment/soil layers and the overlying water column. In addition, the coupling of the phytoplankton model within the nutrient dynamics model allowed for phytoplankton to respond via composition and biomass to nutrient enrichment and changes in salinity regimes. Integrating the nutrient dynamic model with a morphodynamic model also allows for investigating the impact of climate change (e.g. sea level rise and subsidence) and the associated increase in salinities and temperature on the ecological characteristics of these shallow coastal systems. Future improvements to the nutrient dynamics model include better representation of Chl-a, NH4, TSS, TP, and PO4 concentrations that will likely require additional studies of the boundary conditions offshore, point and non-point sources, fluxes through the estuarine passes, as well as atmospheric deposition of nutrients.

4.3. Vegetation dynamic component

The vegetation models were parameterized through field observations and an extensive review of the literature. Integration the vegetation models allowed for predicting reasonable patterns of species distribution, composition, and seasonal biomass dynamics driven by nutrients and hydrodynamics. Overall, the predicted aboveground biomass results are encouraging. The comparison for sites CRMS0135 and 4529 (Fig. 15) suggests that the biomass predictions made by the collective action of the three vegetation models (species distribution, biomass, and biomass allocation) are consistent with the dynamics of the natural ecosystem. At these two locations, the dominant species identified by the model was consistent with observed results. This suggests that the species distribution predicted by vegetation species distribution model, the biomass predicted by vegetation biomass model, and the allocation of biomass to aboveground predicted by vegetation biomass allocation model are individually and collectively reasonable. While these comparisons do provide insight into performance of the models, they must be interpreted with a degree of caution. The spatial scale of data collection from the CRMS sites was not completely compatible with the predictions of the model. The data was collected from a single $0.25\,m^2$ quadrat, while the models are predicting vegetation dynamics at a $0.25\,km^2$ resolution. Therefore, the model often predicts that a location contains several species. On the other hand, a single $0.25\,m^2$ field quadrat was not likely to reflect the full diversity in plants found near the plot. Future work on the vegetation modeling might also include the responses of belowground biomass to wetland soil strength to help better understand how nutrient enrichment might influence erosional properties (Morris et al., 2013; Turner, 2011).

The Integrated Biophysical Model presented here compares well with observations, and captures the seasonal patterns of key processes. There are still discrepancies between modeled and observed data that will require further improvements on how the various processes interact. we recognize the temporal scales of the different components. For example, only the morphodynamics component is accelerated (given the large time scale of sediment processes) while the nutrient dynamics, hydrodynamics, and vegetation dynamics were simulated without the acceleration factor. Periodically, feedbacks among the components were conducted to capture the collective changes to the landscape. A sensitivity analysis was conducted on the appropriate acceleration factor to ensure that the morphologic processes were not altered. Strategic long-term data collection is also needed to better understand the temporal and spatial scales and feedback among these key processes. For example, more measurements are needed to improve the ability of the model to accurately represent how live vegetation

Table 14
Vegetation aboveground (AG) and belowground biomass (BG) comparison between model and observed data in Barataria (n = 12) and Breton (n = 12) basins.

Year	Basin	Biomass	Mean Observed (g C m^{-2})	Mean Modeled (g C m^{-2})	Bias (g C m^{-2})	Std. (g C m^{-2})	RMSE (g C m^{-2})
2014	Barataria	AG	391	101	−290	173.7	83.4
		BG	1351	167	−1184	693.4	96.6
	Breton	AG	489	201	−288	182.1	64.9
		BG	1400	325	−1074	696.4	86.9

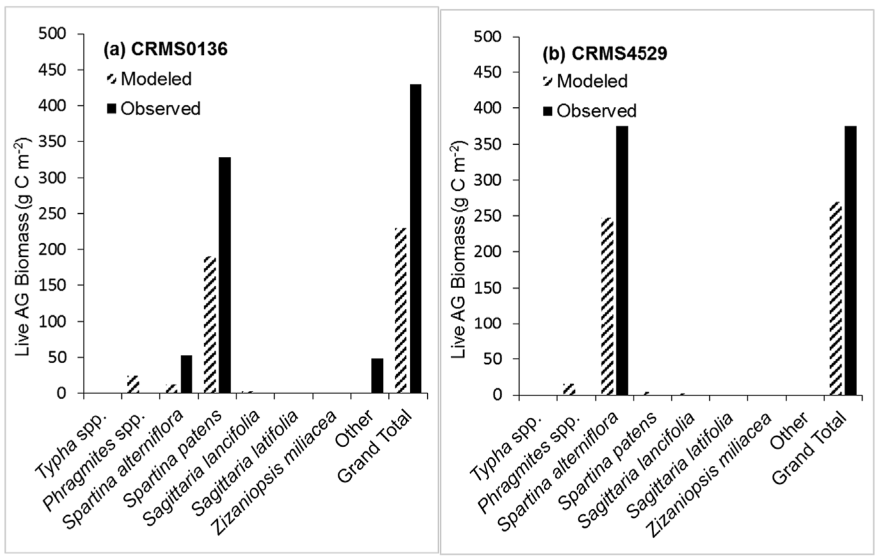

Fig. 15. Aboveground biomass comparison for each of the marsh vegetation taxa, including the grand total at two sites, a) CRMS0136 and b) CRMS4529 for year 2014.

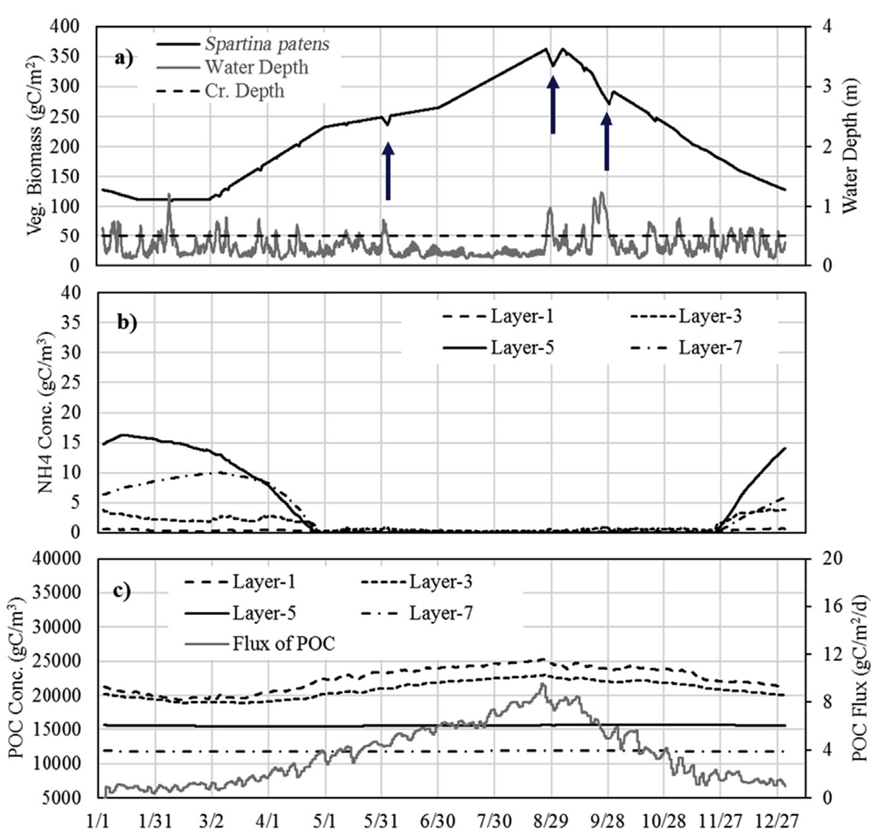

Fig. 16. The modeled response of a) *S. patens* aboveground biomass (from the vegetation biomass model) to variability in the water level (produced from the hydrodynamics model) b) soil porewater ammonium depletion (from the nutrient dynamics model) during the growing season, and c) soil particulate organic carbon fluxes to the top soil layers at site CRMS3985 (see Fig. 6). Arrows in panel a) refer to vegetation biomass responses when the critical water depth was exceeded.

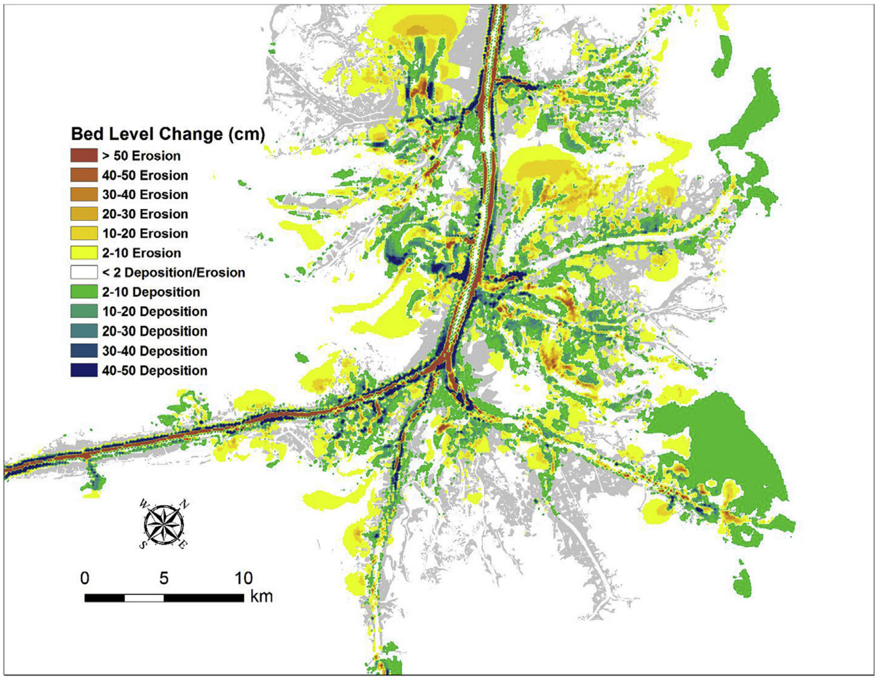

Fig. 17. Difference map of bed levels (hot colors are deposition and cold colors are erosion) of the Mississippi River Bird's Foot Delta and the receiving basins based from a simulation experiment with and without marsh vegetation. (For interpretation of the references to color in this figure legend, the reader is referred to the Web version of this article.)

biomass is influenced by inundation, the rate of biomass loss due to inundation, how vegetation stem density affects sediment trapping, how nutrient loading influences the vegetation above- and below-ground biomass, and how the morphology of the landscape might be altered by these processes.

5. Conclusions

Integrated ecosystem models are advancing to encompass more of the complexity of natural resources because of a demand to better represent ecosystems and projected future conditions and processes. Of especial importance is capturing feedback among hydrodynamics, nutrient dynamics, vegetation dynamics and morphodynamics processes. Such transfer of information back and forth, results in a better representation of ecosystems as a whole but have not been well developed. For example, various hydrodynamic and water quality models representing coastal systems often lack the integration of vegetation dynamics and morphodynamics components. Static assumptions are often made when the other components are missing, such as either ignoring the temporal changes that would influence ecosystem processes or over- or under-estimating how the ecosystem responds to related environmental drivers. The Integrated Biophysical Model presented here advances the field of integrated ecosystem modeling by capturing these essential processes in coastal and deltaic systems that are often undergoing rapid change and need large scale restoration. The model shows how salinity and water level variability affect the spatial distribution of vegetation taxa; how inundation influences the vegetation biomass; how the presence of vegetation results in added flow resistance and potential trapping of mineral sediment; how organic matter accretion and mineral sediment deposition sustains wetlands; how nutrients availability/limitation affect the growth; and how hydrodynamic forcings could cause wetland loss through erosion processes. This integrated model can be a valuable tool to decision makers worldwide who are planning large scale coastal and deltaic restoration projects.

Software availability

Name: Integrated Biophysical Model within Delft3D framework.

Developers: Ehab Meselhe, Melissa M. Baustian, Hoonshin Jung, Scott M. Duke-Sylvester, Jenneke Visser, Dirk Sebastiaan van Maren, Johannes Smits, Valesca Harezlak, Michelle Jeuken.

Contact information: emeselhe@thewaterinstitute.org.

Hardware required: General-purpose computer.

Software required: MPICH2, Microsoft Visual Studio 2010 and Intel Fortran Complier 11.1 (or higher), Python.

Programming language: Fortran 90, Python, C++

Availability: The models are open-source and can be accessed via the repository of Deltares (http://oss.deltares.nl/). Contact the developers for details.

Acknowledgements

This work was supported by Louisiana Coastal Protection and Restoration Authority (CPRA) under the Mississippi River Hydrodynamic and Delta Management Study (under Task Order 27.1). The CPRA Project Team provided guidance on the scope of work, which included: A. Freeman, A. Feldbaum, B.Vosburg, C. Parsons Richards, D. Lindquist, E. Haywood, E. Davoli, E. Jarrell, J. Pahl, J. Wray, J. Favorite, J. Mouton, J. Leblanc, S. Khalil, K. Bollfrass, A. Howard, R. Raynie, B. Gossman, J. Troutman, J. Merrifield, K. Guillory, M. Leadon, M. Turner, S. Langlois, M. Coner, R. Simoneaux, J. Boudreaux, B. Lezina, L. Sharp, and B. Haase.

Acknowledgement goes to A. Khadka, J. Smits, and V. Harezlak for assistance in developing the model components. Thank you to the topical experts, D. Justic (ecosystem modeling), J. White (biogeochemistry), and M. Hester (coastal vegetation ecology) who attended work sessions to provide technical input on the data collection efforts as well as the modeling set up, development, and calibration and validation. Collecting and processing field and laboratory data required the assistance from many individuals including: C. Perry (Gulf South Research Corporation), A. Starr, J. Mathurin (Louisiana State University [LSU]), E. Jarrell, A. Freeman, A. Feldbaum (CPRA), T. Carruthers, B. Yuill, K. Arceneaux, B. Thompson, D. Henson, K. Vernon, S. Matzke, C. Pinsonat, J. Heaton, R. Clark, A. Hijuelos, S. Hemmerling, J. Butler, J. Pereira, B. Garfield, A. Owens, K. Darnell, B. Roth, J. Roberts (The Water Institute of the Gulf), D. Di Leonardo, M. Ramirez, D. Stephens, A. Cuesta, and C. Esposito (Tulane University). Acknowledgement for providing background bathymetry data for planning purposes goes to Moffatt & Nichol, Lake Pontchartrain Basin Foundation (LPBF), and Thad Pratt from the U.S. Army Corps of Engineers (USACE) Engineering Research and Development Center – Coastal Hydraulics Laboratory (ERDC – CHL). Much appreciation goes to S. Piazza (U.S. Geological Survey [USGS]), D. Weifenbach (CPRA), and M. Comeaux (USGS) for providing information about the Coastwide Reference Monitoring System (CRMS) wetlands sites including querying the dominant marsh vegetation for determination of which CRMS sites to collect vegetation and soil samples. Acknowledgement goes to the many landowners in the region that gave us permission to sample on their land and to access their canals for the various data collection tasks. Boat services provided by A. Daugereaux (The Ecology Center, University of Louisiana in Lafayette [ULL]), M. Farizo (Delacroix Corporation), and Louisiana Universities Marine Consortium (LUMCON) assisted in reaching some of the wetland and estuarine open water sites. The authors thank D. Reed, K. Costanza, T. Carruthers, K. Darnell, K. Hastings, T. Kimball, P. LaFargue, and D. Weathers for reviewing earlier drafts and anonymous reviewers for excellent input that strengthened this manuscript.

Appendix A. Supplementary data

Supplementary data related to this article can be found at https://doi.org/10.1016/j.envsoft.2018.05.019.

Supplementary video related to this article can be found at https://doi.org/10.1016/j.envsoft.2018.05.019.

References

Adams, J.B., Bate, G.C., 1999. Growth and photosynthetic performance of *Phragmites australis* in estuarine waters: a field and experimental evaluation. Aquat. Bot. 64, 359–367.
Allison, M.A., Vosburg, B.M., Ramirez, M.T., Meselhe, E.A., 2013. Mississippi River channel response to the Bonnet Carré Spillway opening in the 2011 flood and its implications for the design and operation of river diversions. J. Hydrol. 477, 104–118.
Alizad, K., Hagen, S.C., Morris, J.T., Bacopoulos, P., Bilskie, M.V., Weishampel, J.F., Medeiros, S.C., 2016. A coupled, two-dimensional hydrodynamic-marsh model with biological feedback. Ecol. Model. 327, 29–43. https://doi.org/10.1016/j.ecolmodel.2016.01.013.
Allison, M.A., Demas, C.R., Ebersole, B.A., Kleiss, B.A., Little, C.D., Meselhe, E.A., Powell, N.J., Pratt, T.C., Vosburg, B.M., 2012. A water and sediment budget for the lower Mississippi–Atchafalaya River in flood years 2008–2010: implications for sediment discharge to the oceans and coastal restoration in Louisiana. J. Hydrol 432–433, 84–97. https://doi.org/10.1016/j.jhydrol.2012.02.020.
Anderson, D.M., Glibert, P.M., Burkholder, J.M., 2002. Harmful algal blooms and eutrophication: nutrient sources, composition and consequences. Estuaries 25, 704–726.
Ariathurai, R., Arulanandan, K., 1978. Erosion rates of cohesive soils. J. Hydraul. Eng. 104, 279–283.
Aronson, J., Alexander, S., 2013. Ecosystem restoration is now a global priority: time to roll up our sleeves. Restor. Ecol. 21, 293–296. https://doi.org/10.1111/rec.12011.
Asaeda, T., Karunaratne, S., 2000. Dynamic modeling of the growth of *Phragmites australis*: model description. Aquat. Bot. 67, 301–318.
Asaeda, T., Nam, L.H., Hietz, P., Tanaka, N., Karunaratne, S., 2002. Seasonal fluctuations in live and dead biomass of *Phragmites australis* as described by a growth and decomposition model: implications of duration of aerobic conditions for litter mineralization and sedimentation. Aquat. Bot. 73, 223–239.
Baptist, M.J., Babovic, V., Rodríguez Uthurburu, J., Keijzer, M., Uittenbogaard, R.E., Mynett, A., Verwey, A., 2007. On inducing equations for vegetation resistance. J. Hydraul. Res. 45, 435–450. https://doi.org/10.1080/00221686.2007.9521778.
Barbier, E.B., Hacker, S.D., Kennedy, C., Koch, E.W., Stier, A.C., Silliman, B.R., 2011. The value of estuarine and coastal ecosystem services. Ecol. Monogr. 81, 169–193.
Bertness, M.D., 1991. Zonation of *Spartina patens* and *Spartina alterniflora* in new England salt marsh. Ecology 72, 138–148. https://doi.org/10.2307/1938909.
Bertness, M.D., 1985. Fiddler crab regulation of *Spartina alterniflora* production on a New England salt marsh. Ecology 66, 1042–1055. https://doi.org/10.2307/1940564.
Best, E.P., Boyd, W.A., Kenow, K.P., 2011. A Generic Modeling Approach to Biomass Dynamics of *Sagittaria latifolia* and *Spartina alterniflora* (ERDC TN-SWWRP No. 0704–0188). U.S. Army Engineer Research and Development Center, Vicksburg, MS.
Bianchi, T.S., Allison, M.A., 2009. Large-river delta-front estuaries as natural "recorders" of global environmental change. Proc. Natl. Acad. Sci. 106, 8085–8092. https://doi.org/10.1073/pnas.0812878106.
Birch, J.B., Cooley, J.L., 1982. Production and standing crop patterns of giant cutgrass (*Zizaniopsis miliacea*) in a freshwater tidal marsh. Oecologia 52, 230–235.
Boesch, D.F., 2006. Scientific requirements for ecosystem-based management in the restoration of the Chesapeake Bay and coastal Louisiana. Ecol. Eng. 26, 6–26.
Brouwer, J., 1962. Nutritive influence on the distribution of dry matter in plants. Neth. J. Agric. Sci. 10, 399–408.
Caffrey, J.M., Day, J.W., 1986. Control of the variability of nutrients and suspended sediments in a Gulf Coast estuary by climatic forcing and spring discharge of the Atchafalaya River. Estuaries 9, 295–300.
Calmon, M., Brancalion, P.H.S., Paese, A., Aronson, J., Castro, P., da Silva, S.C., Rodrigues, R.R., 2011. Emerging threats and opportunities for large-scale ecological restoration in the Atlantic forest of Brazil. Restor. Ecol. 19, 154–158. https://doi.org/10.1111/j.1526-100X.2011.00772.x.
Coastal Protection and Restoration Authority of Louisiana, 2012. Louisiana's Comprehensive Master Plan for a Sustainable Coast. Coastal Protection and Restoration Authority of Louisiana, Baton Rouge, LA.
Collins, D.B.G., Bras, R.L., Tucker, G.E., 2004. Modeling the effects of vegetation-erosion coupling on landscape evolution. J. Geophys. Res. Earth Surf 109, F03004. https://doi.org/10.1029/2003JF000028.
Couvillion, B.R., Barras, J.A., Steyer, G.D., Sleavin, W., Fischer, M., Beck, H., Trahan, N., Griffin, B., Heckman, D., 2011. Land Area Change in Coastal Louisiana from 1932 to 2010 (Scientific Investigations Map No. 3164). U.S. Geological Survey.
D'Alpaos, A., Lanzoni, S., Mudd, S.M., Fagherazzi, S., 2006. Modeling the influence of hydroperiod and vegetation on the cross-sectional formation of tidal channels. Estuar. Coast Shelf Sci. 69, 311–324. https://doi.org/10.1016/j.ecss.2006.05.002.
Das, A., Justic, D., Swenson, E., Turner, R.E., Inoue, M., Park, D., 2011. Coastal land loss and hypoxia: the 'outwelling' hypothesis revisited. Environ. Res. Lett. 6, 025001. https://doi.org/10.1088/1748-9326/6/2/025001.
Deegan, L.A., Johnson, D.S., Warren, R.S., Peterson, B.J., Fleeger, J.W., Fagherazzi, S., Wollheim, W.M., 2012. Coastal eutrophication as a driver of salt marsh loss. Nature 490, 388–392.
DeLaune, R.D., Buresh, R.J., Patrick Jr., W.H., 1979. Relationship of soil properties to standing crop biomass of *Spartina alterniflora* in a Louisiana marsh. Estuar. Coast Mar. Sci. 8, 477–487.
Diaz, R.J., Rosenberg, R., 2008. Spreading dead zones and consequences for marine ecosystems. Science 321, 926–929. https://doi.org/10.1126/science.1156401.
Douglas, B.C., 1991. Global sea level rise. J. Geophys. Res. Oceans 96, 6981–6992. https://doi.org/10.1029/91JC00064.
Edmonds, D.A., Slingerland, R.L., 2010. Significant effect of sediment cohesion on delta morphology. Nat. Geosci. 3. https://doi.org/10.1038/ngeo730.
Egbert, G.D., Bennett, A.F., Foreman, M.G.G., 1994. TOPEX/POSEIDON tides estimated using a global inverse model. J. Geophys. Res. Oceans 99, 24821–24852. https://doi.org/10.1029/94JC01894.
Fagherazzi, S., Kirwan, M.L., Mudd, S.M., Guntenspergen, G.R., Temmerman, S., D'Alpaos, A., van de Koppel, J., Rybczyk, J.M., Reyes, E., Craft, C., Clough, J., 2012. Numerical models of salt marsh evolution: ecological, geomorphic, and climatic factors. Rev. Geophys. 50, RG1002. https://doi.org/10.1029/2011RG000359.
Fox, A.M., Haller, W.T., 2000. Production and survivorship of the functional stolons of giant cutgrass, *Zizaniopsis miliacea* (Poaceae). Am. J. Bot. 87, 811–818. https://doi.org/10.2307/2656888.
Frost, J.W., Schleicher, T., Craft, C., 2009. Effects of nitrogen and phosphorus additions on primary production and invertebrate densities in a Georgia (USA) tidal freshwater marsh. Wetlands 29, 196–203.
Ganju, N.K., Brush, M.J., Rashleigh, B., Aretxabaleta, A.L., del Barrio, P., Grear, J.S., Harris, L.A., Lake, S.J., McCardell, G., O'Donnell, J., Ralston, D.K., Signell, R.P., Testa, J.M., Vaudrey, J.M.P., 2015. Progress and challenges in coupled hydrodynamic-ecological estuarine modeling. Estuar. Coast 39, 311–332. https://doi.org/10.1007/s12237-015-0011-y.
Gerard, V.A., 1999. Positive interactions between cordgrass, *Spartina alterniflora*, and the brown alga, *Ascophyllum nodosum* ecad *scorpioides*, in a mid-Atlantic coast salt marsh. J. Exp. Mar. Biol. Ecol. 239, 157–164.
Gessner, M.O., 2000. Breakdown and nutrient dynamics of submerged *Phragmites* shoots in the littoral zone of a temperate hardwater lake. Aquat. Bot. 66, 9–20.
Grace, J.B., 1989. Effects of water depth on *Typha latifolia* and *Typha domingensis*. Am. J. Bot. 76, 762–768. https://doi.org/10.2307/2444423.
Gross, M.F., Hardisky, M.A., Wolf, P.L., Klemas, V., 1991. Relationship between above-ground and belowground biomass of *Spartina alterniflora* (smooth cordgrass). Estuaries 14, 180–191. https://doi.org/10.2307/1351692.
Hester, M.W., Mendelssohn, I.A., McKee, K.L., 1996. Intraspecific variation in salt tolerance and morphology in the coastal grass *Spartina patens* (Poaceae). Am. J. Bot. 83, 1521–1527. https://doi.org/10.2307/2445827.
Hilbert, D.W., 1990. Optimization of plant root: shoot ratios and internal nitrogen concentration. Ann. Bot. 66 (1), 91–99.
Hogg, E.H., Wein, R.W., 1988. The contribution of *Typha* components to floating mat buoyancy. Ecology 69 (1025). https://doi.org/10.2307/1941258.
Hooper, D.U., Adair, E.C., Cardinale, B.J., Byrnes, J.E.K., Hungate, B.A., Matulich, K.L., Gonzalez, A., Duffy, J.E., Gamfeldt, L., O'Connor, M.I., 2012. A global synthesis reveals biodiversity loss as a major driver of ecosystem change. Nature. https://doi.org/10.1038/nature11118.
Howard, R.J., Mendelssohn, I.A., 1999. Salinity as a constraint on growth of oligohaline marsh macrophytes. I. Species variation in stress tolerance. Am. J. Bot. 86, 785–794.
IWMI, 2014. International Water Management Institute's World Water and Climate Data Atlas. http://www.iwmi.cgiar.org/resources/world-water-and-climate-atlas/.
Johnson, W.B., Sasser, C.E., Gosselink, J.G., 1985. Succession of vegetation in an evolving river delta, Atchafalaya Bay, Louisiana. J. Ecol. 73, 973–986. https://doi.org/10.2307/2260162.
Ket, W.A., Schubauer-Berigan, J.P., Craft, C.B., 2011. Effects of five years of nitrogen and phosphorus additions on a *Zizaniopsis miliacea* tidal freshwater marsh. Aquat. Bot. 95, 17–23. https://doi.org/10.1016/j.aquabot.2011.03.003.
Lane, R.R., Day Jr., J.W., Marx, B.D., Reyes, E., Hyfield, E., Day, J.N., 2007. The effects of

riverine discharge on temperature, salinity, suspended sediment and chlorophyll a in a Mississippi delta estuary measured using a flow-through system. Estuar. Coast Shelf Sci. 74, 145–154. https://doi.org/doi:10.1016/j.ecss.2007.04.008.
Laursen, K.R., 2004. The Effects of Nutrient Enrichment on the Decomposition of Belowground Organic Matter in a *Sagittaria lancifolia*-dominated Oligohaline Marsh (Unpublished master's thesis). Louisiana State University: Agricultural and Mechanical College.
Lesser, G.R., Roelvink, J.A., van Kester, J.A.T.M., Stelling, G.S., 2004. Development and validation of a three-dimensional morphological model. Coast Eng. 51, 883–915. https://doi.org/10.1016/j.coastaleng.2004.07.014.
Lorenzen, B., Brix, H., Mendelssohn, I.A., McKee, K.L., Miao, S.L., 2001. Growth, biomass allocation and nutrient use efficiency in *Cladium jamaicense* and *Typha domingensis* as affected by phosphorus and oxygen availability. Aquat. Bot. 70, 117–133. https://doi.org/10.1016/S0304-3770(01)00155-3.
Los, F.J., Blaas, M., 2010. Complexity, accuracy and practical applicability of different biogeochemical model versions. J. Mar. Syst. 81, 44–74. https://doi.org/10.1016/j.jmarsys.2009.12.011.
Los, H., 2009. Eco-hydrodynamic Modelling of Primary Production in Coastal Waters and Lakes Using BLOOM. Wageningen University, Hoogleraar Aquatische Ecologie en Waterkwaliteitsbeheer.
Lü, Y., Fu, B., Feng, X., Zeng, Y., Liu, Y., Chang, R., Sun, G., Wu, B., 2012. A policy-driven large scale ecological restoration: quantifying ecosystem services changes in the Loess Plateau of China. PLoS One 7, e31782. https://doi.org/10.1371/journal.pone.0031782.
Lundberg, C.J., Lane, R.R., Day, J.W., 2014. Spatial and temporal variations in nutrients and water-quality parameters in the Mississippi River-influenced Breton Sound estuary. J. Coast Res. 30, 328–336. https://doi.org/10.2112/JCOASTRES-D-12-00015.1.
McConnaughay, K.D.M., Coleman, J.S., 1999. Biomass allocation in plants: Ontogeny or optimality? A test along three resource gradients. Ecology 80 (8), 2581–2593.
Mendelssohn, I.A., McKee, K.L., Patrick, W.H., 1981. Oxygen deficiency in *Spartina alterniflora* roots: metabolic adaptation to anoxia. Science 214, 439–441.
Meselhe, E., Baustian, M.M., Allison, M. (Eds.), 2015. Basin Wide Model Development for the Louisiana Coastal Area Mississippi River Hydrodynamic and Delta Management Study. The Water Institute of the Gulf Funded by the Coastal Protection and Restoration Authority under Task Order 27.1, Baton Rouge, LA.
Meselhe, E.A., Rodrigue, M.D., 2013. Models Performance Assessment Metrics and Uncertainity Analysis, Louisiana Coastal Area Program Mississippi River Hydrodynamics and Delta Management Study. Louisiana Coastal Area Program, Baton Rouge, LA.
Morris, J.T., Shaffer, G.P., Nyman, J.A., 2013. Brinson Review: perspectives on the influence of nutrients on the sustainability of coastal wetlands. Wetlands 33, 975–988. https://doi.org/10.1007/s13157-013-0480-3.
Negrin, V.L., Villalobos, A.Ede, Trilla, G.G., Botté, S.E., Marcovecchio, J.E., 2012. Above- and belowground biomass and nutrient pools of *Spartina alterniflora* (smooth cordgrass) in a South American salt marsh. Chem. Ecol. 28, 391–404. https://doi.org/10.1080/02757540.2012.666529.
Nicholls, R.J., 2004. Coastal flooding and wetland loss in the 21st century: changes under the SRES climate and socio-economic scenarios. Global Environ. Change 14, 69–86.
Osgood, D.T., Zieman, J.C., 1993. Factors controlling aboveground *Spartina alterniflora* (smooth cordgrass) tissue element composition and production in different-age barrier island marshes. Estuaries 16, 815–826.
Pianosi, F., Beven, K., Freer, J., Hall, J.W., Rougier, J., Stephenson, D.B., Wagener, T., 2016. Sensitivity analysis of environmental models: a systematic review with practical workflow. Environ. Model. Software 79, 214–232. https://doi.org/10.1016/j.envsoft.2016.02.008.
Qualls, R.G., Richardson, C.J., 2000. Phosphorus enrichment affects litter decomposition, immobilization, and soil microbial phosphorus in wetland mesocosms. Soil Sci. Soc. Am. J. 64, 799–808.
Rabalais, N.N., Turner, R.E., Díaz, R.J., Justić, D., 2009. Global change and eutrophication of coastal waters. ICES J. Mar. Sci. J. Cons. 66, 1528–1537.
Ranasinghe, R.W.M.R.J.B., Swinkels, C., Luijendijk, A.P., Bosboom, J., Roelvink, D., Stive, M.J.F., Walstra, D.J.R., 2010. Morphodynamic upscaling with the MORFAC approach. In: 32nd International Conference on Coastal Engineering, ICCE 2010, June 30 – July 5 2010, Shanghai, China, . https://doi.org/10.1016/j.coastaleng.2011.03.010.
Reis, S., Seto, E., Northcross, A., Quinn, N.W.T., Convertino, M., Jones, R.L., Maier, H.R., Schlink, U., Steinle, S., Vieno, M., Wimberly, M.C., 2015. Integrating modelling and smart sensors for environmental and human health. Environ. Model. Software 74, 238–246. https://doi.org/10.1016/j.envsoft.2015.06.003.
Ren, L., Rabalais, N.N., Turner, R.E., Morrison, W., Mendenhall, W., 2009. Nutrient limitation on phytoplankton growth in the upper Barataria Basin, Louisiana: microcosm bioassays. Estuar. Coast 32, 958–974. https://doi.org/10.1007/s12237-009-9174-8.
Reyes, E., White, M.L., Martin, J.F., Kemp, G.P., Day, J.W., Aravamuthan, V., 2000. Landscape modeling of coastal habitat change in the Mississippi delta. Ecology 81, 2331–2349. https://doi.org/10.1890/0012-9658(2000)081[2331:LMOCHC]2.0.CO;2.
Reynolds, J.F., Thornley, J.H.M., 1982. A shoot:root partitioning model. Ann. Bot. 49 (5), 585–597.
Richards, J.H., Ivey, C.T., 2004. Morphological plasticity of *Sagittaria lancifolia* in response to phosphorus. Aquat. Bot. 80, 53–67. https://doi.org/10.1016/j.aquabot.2004.07.004.
Roelvink, J.A., 2006. Coastal morphodynamic evolution techniques. Coast Eng. 53, 277–287. https://doi.org/10.1016/j.coastaleng.2005.10.015.
Savchuk, O.P., Gustafsson, B.G., Müller-Karulis, B., 2012. BALTSEM: a marine model for decision support within the Baltic Sea Region. Balt. Nest Inst. Tech. Rep. 55.
Scheffer, M., Carpenter, S., Foley, J.A., Folke, C., Walker, B., 2001. Catastrophic shifts in ecosystems. Nature 413, 591–596. https://doi.org/10.1038/35098000.
Smits, J., 2013. Delft3D-ECO. Deltares, The Netherlands.
Smits, J.G.C., van Beek, J.K.L., 2013. ECO: a generic eutrophication model including comprehensive sediment-water interaction. PLoS One 8, e68104. https://doi.org/10.1371/journal.pone.0068104.
Soetaert, K., Hoffmann, M., Meire, P., Starink, M., Oevelen, D., van Regenmortel, S.V., Cox, T., 2004. Modeling growth and carbon allocation in two reed beds (*Phragmites australis*) in the Scheldt estuary. Aquat. Bot. 79, 211–234. https://doi.org/10.1016/j.aquabot.2004.02.001.
Stanley, D.J., Warne, A.G., Dunbar, J.B., 1996. Eastern Mississippi Delta: late Wisconsin unconformity, overlying transgressive facies, sea level and subsidence. Eng. Geol. 45, 359–381. https://doi.org/10.1016/S0013-7952(96)00022-1.
Stanton, L.E., 2005. The Establishment, Expansion and Ecosystem Effects of *Phragmites australis*, an Invasive Species in Coastal Louisiana. Louisiana State University.
Stutzenbaker, C.D., 2010. Aquatic and Wetland Plants of the Western Gulf Coast. Texas A &M University Press, College Station, Texas, USA.
Syvitski, J.P.M., Kettner, A.J., Overeem, I., Hutton, E.W.H., Hannon, M.T., Brakenridge, G.R., Day, J., Vörösmarty, C., Saito, Y., Giosan, L., Nicholls, R.J., 2009. Sinking deltas due to human activities. Nat. Geosci. 2, 681–686. https://doi.org/10.1038/ngeo629.
Syvitski, J.P.M., Vorosmarty, C.J., Kettner, A.J., Green, P., 2005. Impact of humans on the flux of terrestrial sediment to the global coastal ocean. Science 308, 376–380. https://doi.org/10.1126/science.1109454.
Thornley, J.H.M., 1972. A balanced quantitative model for root: shoot ratios in vegetative plants. Ann. Bot. 36 (2), 431–441.
Turner, R.E., 2011. Beneath the salt marsh canopy: loss of soil strength with increasing nutrient loads. Estuar. Coast 34, 1084–1093. https://doi.org/10.1007/s12237-010-9341-y.
Turner, R.E., Rabalais, N.N., 1991. Changes in Mississippi River water quality this century. Bioscience 41, 140–147.
Tweel, A.W., Turner, R.E., 2012. Watershed land use and river engineering drive wetland formation and loss in the Mississippi River birdfoot delta. Limnol. Oceanogr. 57, 18–28. https://doi.org/10.4319/lo.2012.57.1.0018.
van der Wegen, M., Wang, Z.B., Savenije, H.H.G., Roelvink, J.A., 2008. Long-term morphodynamic evolution and energy dissipation in a coastal plain, tidal embayment. J. Geophys. Res. Earth Surf 113 n/a-n/a. https://doi.org/10.1029/2007JF000898.
van Maren, D.S., Cronin, K., 2016. Uncertainty in complex three-dimensional sediment transport models: equifinality in a model application of the Ems Estuary, The Netherlands. Ocean Dynam. https://doi.org/10.1007/s10236-016-1000-9.
van Rijn, L.C., 2007a. Unified view of sediment transport by currents and waves. I: initiation of motion, bed roughness, and bed-load transport. J. Hydraul. Eng. 133, 649–667. https://doi.org/10.1061/(ASCE)0733-9429(2007)133:6(649).
van Rijn, L.C., 2007b. Unified view of sediment transport by currents and waves. II: suspended transport. J. Hydraul. Eng. 133, 668–689. https://doi.org/10.1061/(ASCE)0733-9429(2007)133:6(668).
Visser, J., Duke-Sylvester, S., 2017. LaVegMod V2: modeling coastal vegetation dynamics in response to proposed coastal restoration and protection projects in Louisiana, USA. Sustainability 9 (1625). https://doi.org/10.3390/su9091625.
Visser, J.M., Duke-Sylvester, S.M., Carter, J., Broussard, W.P., 2013. A computer model to forecast wetland vegetation changes resulting from restoration and protection in coastal Louisiana. J. Coast Res. 67, 51–59. https://doi.org/10.2112/SI_67_4.
Walling, D.E., Fang, D., 2003. Recent trends in the suspended sediment loads of the world's rivers. Global Planet. Change 39, 111–126. https://doi.org/10.1016/S0921-8181(03)00020-1.
Wang, H., Chen, Q., Hu, K., La Peyre, M.K., 2016. A modeling study of the impacts of Mississippi River diversion and sea-level rise on water quality of a deltaic estuary. Estuar. Coast. https://doi.org/10.1007/s12237-016-0197-7.
Weisner, S.E.B., Miao, S.L., 2004. Use of morphological variability in *Cladium jamaicense* and *Typha domingensis* to understand vegetation changes in an Everglades marsh. Aquat. Bot. 78, 319–335. https://doi.org/10.1016/j.aquabot.2003.11.007.
Wolanski, E., Elliot, M., 2015. Estuarine Ecohydrology: an Introduction, second ed. Elsevier.
Yuill, B.T., Khadka, A.K., Pereira, J., Allison, M.A., Meselhe, E.A., 2016. Morphodynamics of the erosional phase of crevasse-splay evolution and implications for river sediment diversion function. Geomorphology 259, 12–29. https://doi.org/10.1016/j.geomorph.2016.02.005.Further reading
Holling, C.S., 1959. The components of predation as revealed by a study of small-mammal predation of the European pine sawfly. Can. Entomol. 91, 293–320.